catalysts

MDPI

Review

Critical Issues and Guidelines to Improve the Performance of Photocatalytic Polymeric Membranes

Marta Romay, Nazely Diban, Maria J. Rivero, Ane Urtiaga and Inmaculada Ortiz *

Department of Chemical and Biomolecular Engineering, ETSIIyT, University of Cantabria Avda. Los Castros s/n, 39005 Santander, Spain; romaym@unican.es (M.R.); dibann@unican.es (N.D.); mariajose.rivero@unican.es (M.J.R.); urtiaga@unican.es (A.U.)

* Correspondence: ortizi@unican.es; Tel.: +34-942-201-585

Received: 29 April 2020; Accepted: 17 May 2020; Published: 19 May 2020

Abstract: Photocatalytic membrane reactors (PMR), with immobilized photocatalysts, play an important role in process intensification strategies; this approach offers a simple solution to the typical catalyst recovery problem of photocatalytic processes and, by simultaneous filtration and photocatalysis of the aqueous streams, facilitates clean water production in a single unit. The synthesis of polymer photocatalytic membranes has been widely explored, while studies focused on ceramic photocatalytic membranes represent a minority. However, previous reports have identified that the successful synthesis of polymeric photocatalytic membranes still faces certain challenges that demand further research, e.g., (i) reduced photocatalytic activity, (ii) photocatalyst stability, and (iii) membrane aging, to achieve technological competitiveness with respect to suspended photocatalytic systems. The novelty of this review is to go a step further to preceding literature by first, critically analyzing the factors behind these major limitations and second, establishing useful guidelines. This information will help researchers in the field in the selection of the membrane materials and synthesis methodology for a better performance of polymeric photocatalytic membranes with targeted functionality; special attention is focused on factors affecting membrane aging and photocatalyst stability.

Keywords: membrane functionality; persistent organic pollutants; photocatalytic membranes; photocatalytic membrane reactor (PMR); composite polymeric membranes; wastewater treatment

1. Introduction

The wide use of chemicals in our society contributes to the accumulation of a huge amount of pollutants in the environment. Many of these recalcitrant pollutants listed in the Stockholm Convention on Persistent Organic Pollutants (POPs) [1] are persistent in the environment due to their strong and stable structure; therefore, conventional technologies of wastewater treatment are not able to degrade or remove them [2].

Advanced oxidation processes are based on the degradation of organic or inorganic contaminants in water and wastewater through oxidation reactions. Among all, heterogeneous photocatalysis is a promising technology in the field of environmental applications because it is driven by UV or visible light [3,4]. Photocatalysis needs a semiconductor material that is excited mainly with UV light. Oxidant species produced during the photocatalytic process can attack the pollutant and break the molecule in smaller compounds. The main advantages of the photocatalytic technology are (i) low operational and installation costs and null post-treatment cost as there is no sludge production except in suspended systems, (ii) it is a technology capable of degrading non-biodegradable pollutants, and (iii) advances in the development of new composite photocatalysts, by doping the primary semiconductor with a co-catalyst, could open up the possibility to use low-cost visible light. However, among certain

drawbacks it is worth mentioning the short service life and high power consumption of the light source, and the requirement of a facility for the photocatalyst recovery in suspended systems [3].

Hybrid processes, such as photocatalytic membrane reactors, PMRs, integrate the activity of the photocatalyst and membrane separation in the same device, this configuration shows great potential to effectively solve the separation problem of harsh systems and the recovery of the catalyst particles in wastewater treatment. Thus, PMRs not only maintain the advantages of photocatalyst technology for degrading high concentration of refractory organic wastes, but they also have the benefit of non-selectivity, fast reaction speed, and complete degradation [5].

Furthermore, the potential harmful effects of nanoparticles are still under debate. If they are not correctly handled and they are released to the environment, they could interact with living organisms. They have similar dimensions to biological molecules such as proteins, so they can enter the human body. Small concentrations of about 5–50 μg/L may cause physiological changes, chromosomal alterations and oxidative stress [6]. Photocatalyst immobilization on membranes can significantly contribute to avoid nanoparticles hazards.

Different classifications have been followed to better characterize PMRs [7–9]. The first one distinguishes between the catalyst being suspended in solution (SPMR) and the catalyst being immobilized on the membrane (IPMR). SPMR primarily aimed at catalyst separation and recovery. The membrane can be submerged in the photocatalytic reactor, Figure 1A [10]. This configuration fails from protecting the membrane for UV irradiation after long operation times (Figure 1AI), although this effect could be reduced with the use of a light-tight baffle in between the light source and the membrane (Figure 1AII). Alternatively, the membrane can be placed out of the photo-reactor, Figure 1B [10], but this configuration is prone to higher pressure drops in the catalyst flow and instability of the catalyst concentration inside the reactor. Otherwise, the catalysts can be fixed to the membrane, IPMR. In this configuration, the membrane can act as support with the only function of immobilizing the catalyst (Figure 1C), or the membrane can integrate the catalyst and simultaneously have a separation function, Figure 1D,E [10]. In this latter system, the membrane acts both as selective barrier for the contaminants to be degraded, thus maintaining them into the reaction environment, and as the support for the photocatalyst. Here, two different flow configurations are possible, dead-end, Figure 1D; or cross-flow, Figure 1E [7]. External illumination is usually applied for these configurations [5,10].

IPMR configuration is raised as an advanced solution. Although suspension photocatalysis results in great pollutant degradation yields due to the large surface area of the nano-size particles, this is at the same time the main drawback that makes difficult the catalyst separation and recovery. Moreover, nanoparticles tend to agglomerate which can lead to a reduction of the reaction yield. This could be somehow avoided if they are properly fixed to some supporting material as it is promoted in IPMRs. In addition, membrane fouling in SPMRs due to photocatalyst deposition is an additional problem. In line with a process intensification philosophy, photocatalyst immobilization can avoid the necessity of the photocatalyst post-recovery stage. Furthermore, it could simultaneously overcome fouling phenomena associated with the photocatalyst and pollutants [4,5,8].

In advanced IPMRs, the role of the membrane is to perform as a barrier to retain the pollutants as well as photocatalyst support. The membrane support can be made of ceramic, metallic, or polymeric materials [8]. Although ceramic and metallic membranes have great chemical stability and high mechanical strength, their applications are limited because of the manufacturing costs [4,8]. Taking into account the economic factor, polymeric membranes are cheaper and easier to apply on an industrial scale in spite of their limitations. Moreover, they are easy to process, and their properties and microstructure can be tuned. The selection of the polymeric membrane material is not trivial. Due to the nature of polymers as long-chain carbon molecules, they are susceptible to UV light and oxidative species degradation that can damage the membrane during the photocatalytic process. The challenge is to develop low-cost polymeric membranes with adequate mechanical strength and flexibility, which withstand UV and oxidative conditions [4] while supporting the photocatalyst particles. Furthermore,

the conformed polymeric membrane should prevent the pollutant from crossing the membrane before photocatalytic degradation while still performing with sufficiently high total flux.

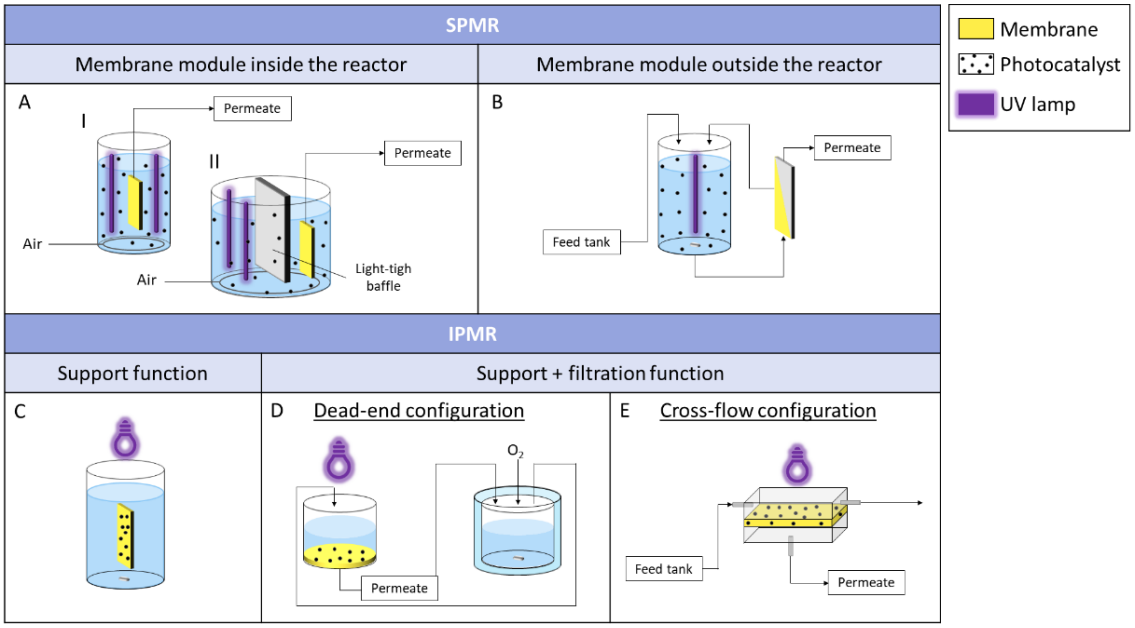

Figure 1. Photocatalytic membrane reactor configurations A and B suspended in solution photocatalytic membrane reactors (SPMR), (**A**): Membrane module inside the reactor; (**B**): Membrane module outside the reactor; (**C**–**E**) immobilized in a membrane photocatalytic membrane reactors (IPMR) C: a membrane with support function; D (dead-end configuration) and E (cross-flow configuration) of a membrane with simultaneous support and filtration function. Adapted from [7,10].

Previous reviews [11–14] have addressed the most recent advances on membrane synthesis and applications and have detected major challenges that need to be overcome to develop technically competitive IPMRs for future scaling-up and expansion of the technology. One of these challenges results from the intrinsic nature of an immobilized nanoparticle system. The photocatalyst can be immobilized either in the membrane matrix or on the membrane surface as a coating layer. The method of photocatalyst immobilization importantly affects the photocatalyst distribution in the membrane, its stability and accessibility to light-source. Therefore, a rigorous and methodological analysis of how the immobilization method of the photocatalyst in the membrane affects all those parameters needs to be done to ascertain their impact on the overall performance of the functional membrane, in terms of flux properties and photocatalytic activity [4].

This is the first attempt reported in the literature to critically review the information on photocatalytic polymeric membranes so far applied to the treatment of waters and wastewaters polluted with POPs or model organic pollutants; the analysis has been focused to identify the influence of (i) the polymer and photocatalyst selection and, (ii) the methodology of membrane synthesis, on the functional properties of the resulting membranes. As a major novelty, this review is conceived to not only point out the major challenges collected after reviewing the literature, but it also extracts the reasons of current failures and proposes guidelines and solutions to overcome the reported limitations for the successful development of photocatalytic polymeric membranes. Thus, this review aims at becoming a practical guide for scientists in the field of photocatalytic membranes to decide the best methodological approach to deal with the synthesis of new functional photocatalytic membranes and to detect possible experimental gaps that future research would need to fill.

2. Materials in Polymeric Photocatalytic Membranes

Tables 1–3 show a literature survey of the porous photocatalytic polymer membranes synthesized so far. Tables 1 and 2 collect the photocatalytic membranes classified as mixed matrix membranes (MMM), considering that the photocatalyst is dispersed in a polymeric matrix. Table 1 presents the membranes synthesized by phase inversion methods and Table 2 presents the membranes synthesized by electrospinning. On the other hand, Table 3 collects the works that propose different synthesis techniques of thin-film composite membranes (TFCM). Moreover, the materials employed (i.e., polymer, non-solvent, additive, and photocatalyst), components composition and the application evaluated in each study are presented. These data will be analyzed to acquire knowledge to define the guidelines that will help to decide which is the adequate material and processing technique for the desired application.

Table 1. Mixed-matrix membrane systems synthesized by phase inversion: materials, compositions, and applications.

Polymer (wt. %)	Solvent	Non-Solvent	Additive (wt. %)	Photocatalyst	wt.% (Polymeric Solution)	wt. %/cm^2 (Membrane)	Application (Removed Pollutant)	Author
PVDF (20)	DMAc	deionized water	PEG (5)	TiO_2	0–7, 5 *	0–0.612, 0.478 *	BSA	Méricq, J.P [15]
PVDF (20)	DMAc	deionized water	PEG (5)	TiO_2	4	0.30	(-)	Tran, D. [16]
PVDF (19)	DMAc	distilled water	PVP (7)	Ag-TiO_2	0.01-0.06, 0.06 *	(-)	BSA, E.Coli	Chen, Q. [17]
PVDF (18)	DMAc	deionized water	PVP (2)	TiO_2	0–1, 1 *	0–0.33, 0.33 *	Estrone, 17β-estradiol	Wang, M. [18]
PVDF (16)	DMAc	water: isopropanol (70:30)	(-)	TiO_2	0–3, 2*	0–0.04, 0.027	RTB	Sakarkar, S. [19]
PVDF (15)	DMAc	Water	PVP (1)	GO-TiO_2	1	0.32	BSA	Xu, Z [20]
PVDF (15)	DMAc	distilled water	PVP (1)	GO-OMWCNTs	1% (carb/pol)	(-)	BSA	Zhang, J. [21]
PVDF (14)	DMAc	tap water	(-)	AC-TiO_2	(0–0.5)–(0–0.1)	0.106	BSA	Liu, Q. [22]
PVDF (12)	DMAc	tap water	PEG (1–5), 2 *	TiO_2	0.25–2, 0.5 *	0.042–0.297,0.083 *	NOM, HA	Song, H. [23]
PVDF (12)	DMAc	Tap water	LiCl (0–4), 0.5 *	TiO_2	0–1.5, 0.5 *	0–0.23, 0.083 *	NOM, HA	Song, H. [24]
PVDF+PMMA (12)	TEP	Water	PEG (25) + PEG (5)	TiO_2	0–0.5, 0.5 *	0–0.5, 0.5 *	MB	Benhabiles, O. [25]
PVDF (10)	NMP	tap water	(-)	TiO_2	0–4, 2–4 *	0–0.189, 0.110–0.189 *	E. Coli, RB5, BSA	Damodar, R.A. [26]
PMAA-g-PVDF/PAN (-)	DMAc	Ethanol:deionized water (1:3)	(-)	N-TiO_2	1,3,5	(-)	Bentazon	Mungondori, H. [27]
PSF (20)	NMP	distilled water	(-)	TiO_2	0–2.43, 1.96 *	0–0.553, 0.455 *	Cr(VI)	Jyothi, M.S. [28]
PSF (18)	DMAc:NMP	Ethanol:water (20:80)	(-)	TiO_2	0–5, 2 *	(-)	BSA	Yang, Y. [29]
PSF (18)	DMAC:NMP (4:1)	deionized water	PEG (8)	Fe-TiO_2	0–4.5, 3.6 *	0–0.077	BPA	Wang, Q. [30]
PSF (18)	DMAC	Water	(-)	TiO_2-ZnO, TiO_2-SiO_2	0.16	(-)	MO, phenol	El-Aassar, A. [31]
PSF (18)	NMP	deionized water	(-)	N, Pd-TiO_2	0–1.26, (0–7)	(-)	EY	Kuvarega, A.T. [32]
PSF (18)	NMP	Water	PVP (2)	N-rGO-TiO_2	0.5	0.095	DR 80, DB 15	Xu, H. [33]
PSF (17)	NMP	tap water	PVP (0.5)	mpg-C_3N_4-TiO_2	0–1, 1 *	0–0.653, 0.653 *	SMX	Yu, S. [34]
PSF (12)	DMF	distilled water	(-)	CNTs-TiO_2	1	(-)	Ampicillin Erithtomycin	Muhulet, A. [35]

Table 1. *Cont.*

Polymer (wt. %)	Solvent	Non-Solvent	Additive (wt. %)	Photocatalyst	wt.% (Polymeric Solution)	wt. %/cm^2 (Membrane)	Application (Removed Pollutant)	Author
PES (27 g)	DMF, EtOH (1–4)	distilled water	(-)	TiO_2	0.1–0.4, 0.1 *	0.0062–0.024, 0.0062 *	HA	Sotto, A. [36]
PES (26)	NMP	Water	(-)	Co-TiO_2	0.5–1, 1 *	0.065–0.129, 0.129 *	2-DCP	Hoseini, S. N. [37]
PES (21)	DMAc	distilled water	PVP (1)	rGO-TiO_2	0.05–0.2, 0.1 *	0.237–0.943, 0.497 *	DY 12, RG 19, RB 21, BSA	Safarpour, M. [38]
PES (20)	DMAc	distilled water	PVP (1)	B-TiO_2-SiO_2/$CoFe_2O_4$	0–1, 0.5 *	0–0.497, 0.239 *	DR 16, POME	Zangeneh, H. [39]
PES (18)	NMP	tap water	SMM (1)	O-g-C_3N_4	1	(-)	Phenol	Salim, N. [40]
PES (18)	NMP	tap water	SMM (1–5,4 *)	O-g-C_3N_4	1	(-)	Phenol	Salim, N. [41]
PES (15)	DMAc	Water	PVP (5)	mNi-TiO_2	0–1, 1 *	0-0.083, 0.083 *	BSA, YEF, SA, HA, MB	Sun, T. [42]
PES-F-COOH (20)	DMF	deionized water	PVP (10)	TiO_2	1–5,5 *	0.123–0.519, 0.519 *	PAM	Geng, Z. [43]
CA-PS (-)	Acetone	distilled water	(-)	ZnO	0.1 g	(-)	CR, RY 105	Rajeswari, A. [44]
CA-PU (-)	Acetone-chloroform	distilled water	(-)	ZnO	0.3	(-)	RR 11, RO 84	Rajeswari, A. [45]
P(VDF-TrFE) (10)	DMF	(-)	(-)	TiO_2	8	0.32	MB, CIP, IBP	Martins, P.M. [46]
P(VDF-TrFE) (10)	DMF	(-)	(-)	TiO_2	8	0.017	Tartrazine	Aoudjit, L. [47]
P(VDF-TrFE) (10)	DMF	(-)	(-)	TiO_2, ZnO	0–15,15 *	0–3.75, 3.75	MB	Teixeira, S. [48]
P(VDF-TrFE) (10)	DMF	(-)	(-)	TiO_2 (NaY)	0–8, (0–8), 8(8) *	0–3.70, 3.70 *	MB	Martins, P.M. [49]
PVDF-HFP (15)	DMF	(-)	(-)	Ag- TiO_2	0-10, 10 *	0–0.56, 0.56 *	NOR	Salazar, H. [50]
PSF (16)	NMP	distilled water	PVP (2)	TiO_2, MIP TiO_2, NIP TiO_2	2	(-)	MB, MO	Melvin, H.K. [51]
PVDF Dul layer HF (18 in, 15 out)	DMAc	tap water	(-)	TiO_2	0 (in) 3 (out)	(-)	8 pharmaceutical mixture	Paredes, L. [52]
PVDF Dual layer HF (18 in, 15 out)	DMAc	tap water	(-)	TiO_2	0 (in) 3–15 (out), 3 *	0 (in) 0.067–0.201 (out), 0.067 *	NOM	Dzinun, H. [53]

Table 1. *Cont.*

Polymer (wt. %)	Solvent	Non-Solvent	Additive (wt. %)	Photocatalyst	wt.% (Polymeric Solution)	wt. %/cm^2 (Membrane)	Application (Removed Pollutant)	Author
PVDF Dual layer HF (18 in, 15 out)	DMAc	tap water	(-)	TiO_2	0 (in) 3–15 (out)	0 (in) 0.067–0.201 (out)	NP	Dzinun, H. [54]
PVDF Dual layer HF (18 in, 15 out)	DMAc	tap water	(-)	TiO_2	0 (in) 3 (out)	0 (in) 0.067 (out)	NP	Dzinun, H. [55]
PVDF Dual layer HF (18 in, 15 out)	DMAc	tap water	(-)	TiO_2	0 (in) 0–15 (out), 15 *	0 (in) 0–0.201 (out), 0.201 *	NP	Dzinun, H. [56]
PVDF Dual layer HF (18 in, 15 out)	DMAc	tap water	PEG (5 in, 0 out)	TiO_2	0 (in) 3 (out)	0 (in) 0.067 (out)	NP	Dzinun, H. [57]
PVDF HF (18–19)	NMP	tap water	PVP (15) PEG	TiO_2	0.5	0.071	MB	Galiano, F. [58]
PVDF HF (18)	DMAc	Water	PVP (5)	TiO_2	0–4, 2 *	(-)	Oil wastewater	Ong, C.S. [59]
PVDF (18)	DMAc, NMP, DMF	Water	(-)	TiO_2	0.001, 0.01, 0.1 g/L	(-)	HA	Teow, Y.H [60]

* optimal concentration.

Table 2. Mixed-matrix membrane systems synthesized by electrospinning: materials, compositions and application.

Polymer (wt. %)	Solvent	Additive	Photocatalyst	wt. % (Polymeric Solution)	Application (Removed Pollutant)	Author
P(VDF-TrFE) (15)	DMF/MEK, 85/15	(-)	GO-TiO_2	0–20, 5 *	MB	Almeida, N.A. [61]
PVDF (-)	(-)	PEO	TiO_2-MWCNTs (20:1)	0–40	HA	Chen, J. [62]
PTFE: PVA (6:1)	water	PVA	ZnO	0–30, 20 *	RhB	Huang, Y. [63]
PTFE (15)	(-)	PVA (1), BA (0.0025)	TiO_2	(-)	MB	Kang, W. [64]
PA6 (12)	AA: FA (2:1)	(-)	TiO_2	25	*E. coli*, RBB	Blanco, M. [65]
PAN (8)	DMF	(-)	TiO_2-ZnO	2	MG	Yar, A. [66]
PAN (6)	DMF	(-)	ZnO	0.9	MO	Tissera, N. D. [67]
PAN (7)	DMF	(-)	TiO_2	3.57	Nitrate	Suriyaraj, S.P. [68]

* optimal concentration. Abbreviations: Polymers: cellulose acetate (CA), polyamide 6 (PA6), polyacrylonitrile (PAN), polyethersulfone (PES), polystyrene (PS), polysulfone (PSF), polytetrafluoroethylene (PTFE), polytrifluoroethylene (PTrFE), polyurethane (PU), polyvinylidene fluoride (PVDF), PVDF-co-hexafluoropropylene (PVDF-HFP) ; Solvents: acetic acid (AA), dimethylacetamide (DMAc), dimethylformamide (DMF), ethanol (EtOH), formic acid (FA), methyl ethyl ketone (MEK), N-methylpyrrolidone (NMP), triethyl phosphate (TEP); Photocatalysts: activated carbon (AC), silver (Ag), boron (B), bismuth (Bi), carbon nanotubes (CNTs), cobalt (Co), cobalt ferrite ($CoFe_2O_4$), carbon quantum dots (CQDs), iron (Fe), graphene oxide (GO), molecular imprinting polymer (MIP), mesoporous graphitic carbon nitride (mpg-C_3N_4), multi-walled carbon nanotubes (MWCNTs), nitrogen (N), sodium Y zeolite (NaY), magnetic nickel (mNi), non-imprinting polymer (NIP), oxygen doped graphitic carbon nitride (O-g-C_3N_4), oxygenated MWCNTs (OMWCNTs), palladium (Pd), reduce graphene oxide (rGO), silicon oxide (SiO_2), titanium dioxide (TiO_2), zinc oxide (ZnO); Additives: boric acid (BA), lithium chloride (LiCl), polyethylene glycol (PEG), polyethylene oxide (PEO), polyvinyl alcohol (PVA), polyvinyl pyrrolidone (PVP), surface molecule modifier (SMM); Pollutants: 2,4 dichlorophenol (2-DCP), bovine serum albumin (BSA), bisphenol A (BPA), ciprofloxacin (CIP), congo red (CR), direct blue (DB), direct red (DR), direct yellow (DY), *Escherichia coli* (*E. Coli*), eosin yellow (EY), humic acid (HA), ibuprofen (IBP), indigo carmine (IC), methylene blue (MB), malachite green (MG), methylene orange (MO), Natural Organic Matter (NOM), norfloxacin (NOR), nonylphenol (NP), polyacrylamide (PAM), palm oil mill effluent (POME), reactive black 5 (RB5), reactive blue 21 (RB21), Remazol black B (RBB), reactive green (RG), rhodamine B (RhB), reactive orange (RO), reactive red (RR), remazol turquoise blue (RTB), reactive yellow (RY), ammonium alginate (SA), sulfamethoxazole (SMX), yeast extract fermentation (YEF).

Table 3. Literature review on thin film composite membranes: synthesis methods, materials, compositions, and pollutant application.

Synthesis Method	Support Material	A_{eff} (cm^2)	Photocatalyst	Photocatalyst Mass (mg)	Photocatalyst per Membrane Area (mg/cm^2)	Application (Removed Pollutant)	Author
Vacuum deposition	PES (com) Pretreatment: PAAM	4.3	nAg-GO- TiO_2	3	0.697	*E. coli*, *B. subtilis*	Jiang, Y. [69]
Vacuum deposition	CA (com) Pretreatment: PEG + GA	12.56	Ag-rGO- TiO_2	2.5–20, 10 *	0.199–1.59, 0.796 *	MB, RhB, oil water	Chen, Q. [70]
Vacuum deposition	CA (com)	12.56	rGO-g-C_3N_4	10–100, 25 *	0.796–7.96, 1.99 *	RhB	Zhao, H. [71]
Vacuum deposition	MCE (com)	1.54	GO- TiO_2	10	6.49	DP, MO	Pastrana-Martínez, L [72]
Vacuum deposition	PC (com)	(-)	GO- TiO_2	(-)	(-)	DR 80, DB 15	Xu, C. [73]
Vacuum deposition	PC (com)	(-)	GO- TiO_2	(-)	(-)	MO, RhB	Xu, C. [74]
Vacuum deposition (Support: Electrospinning)	PAN (8wt. %, DMF)	12.56	rGO-α-Fe_2O_3	(-)	(-)	MB, MO, RhB, R6G, MG, GV	Sun, K. [75]
Filtration	CA (com)	14.6	GO-TiO_2	50–400, 100 *	3.42–27.4, 6.85 *	CR	Nair, A.K. [76]
Filtration	CA (com)	11.94	GO-TiO_2	50–300, 200 *	4.18–25.12, 16.75 *	RhB, AO7	Gao, P. [77]
Immersion	PSF (com) Pretreatment: PVA (2.5 mg)	17.34	AC-N-rGO-TiO_2	10–160, 120 *	0.57–9.22, 6.92 *	MO	Wu, T. [78]
Immersion (Support: Electrospinning)	CA-GO (15−(0–1.5) wt. %, DMF) Pretratment: GA	(-)	NH_2-TiO_2	0.005 g/mL	(-)	MB, IC	Aboamera, N. M. [79]
Immersion (Support: Electrospinning)	PAN-CNT (10 wt. %, DMF) Pretratment: GA	(-)	NH_2-TiO_2	40.6 wt. % (CNT-TiO_2) NF	(-)	Cr (VI)	Mohamed, A. [80]
Immersion - In situ growth (Support: Electrospinning)	PAN (9 wt. %, DMF) Pretreatment: PDA	20	Ag-TiO_2	(-)	(-)	MB, Phenol	Shi, Y. [81]

Table 3. *Cont.*

Synthesis Method	Support Material	A_{eff} (cm^2)	Photocatalyst	Photocatalyst Mass (mg)	Photocatalyst per Membrane Area (mg/cm^2)	Application (Removed Pollutant)	Author
Immersion (Layer by Layer (LbL))	PSF (com)	(-)	GO-TiO_2	(-)	0.062	MB	Gao, Y. [82]
Immersion (Support: Phase inversion)	PEI/P25 (24/1.23 wt. %, NMP)	12.56	TiO_2 nw	250	19.9	RhB	Jiang, R. [83]
Immersion (Plasma-grafted)	PVDF-g-PAA (com)	4.5	TiO_2	0.5 1.5 3 (% m/v)	(-)	RB5, BSA	You, S.-J. [84]
Immersion (UV-grafted)	PA-g-PAA (com)	13.4	Ag-ZnO-Fe_3O_4-MWCNTs	8.7	0.649	Amoxicilin	Irani, E. [85]
Electrospraying (Support: Electrospinning)	PVDF (18 wt. %, DMF:acetone 60:40)	45	TiO_2	4.5–27, 27 *	0.1–0.6, 0.6 *	BPA, 4-CP, CMT	Ramasundaram, S. [86]
Coaxial electrospinning	PAN (10, 15 core) DMAc	(-)	CQDs-Bi_{20}-TiO_{32}	5, 10, 15 *w/v*%	(-)	Isoproturon	Xie, R. [87]
Hot pressing (Support: Phase inversion)	PVDF (-wt. %, DMAc)	(-)	TiO_2	(-)	(-)	BPA	Nor, N.A.M. [88]
Sputtering + Anodization	PES (com)	17.35	TiO_2	(-)	(-)	diclofenac	Fischer, K. [89]

* Optimal concentration. Abbreviations: Polymers: cellulose acetate (CA), commercial (com), mixed cellulose esters (MCE), polyamide (PA), polyacrylonitrile (PAN), polycarbonate (PC), (polyetherimide (PEI), polyethersulfone (PES), polysulfone (PSF), polyvinylidene fluoride (PVDF); Solvents: dimethylacetamide (DMAc), dimethylformamide (DMF), N-methyl pyrrolidone (NMP). Additives: glutaraldehyde (GA), litium chloride (LiCl), polyacrylic acid (PAA), polyallylamine (PAAM), polyethylene glycol (PEG), polydopamine (PDA), polyvinyl alcohol (PVA); Photocatalysts: activated carbon (AC), silver (Ag), cobalt (Co), graphitic carbon nitride (g-C_3N_4), graphene oxide (GO), nitrogen (N), nano-silver (nAg), amine group (NH_2), nanowire (nw), polyoxometalate (POM), reduce graphene oxide (rGO), titanium dioxide (TiO_2), hematite (α-Fe_2O_3); Pollutant: 4-chlorophenol (4-CP), acid orange 7 (AO7), *Bacillus subtilis* (*B. subtilis*), bisphenol A (BPA), bovine serum albumin (BSA), cimentine (CMT), congo red (CR), chromium VI (Cr VI), crystal violet (CV), direct blue (DB), Diphenhydramine (DP), direct red (DR), *Escherichia coli* (*E. coli*), gentian violet (GV), humic acid (HA), indigo carmine (IC), methylene blue (MB), malachite green (MG), Methyl Orange (MO), reactive black 5 (RB5), rhodamine B (RhB), rhodamine 6G (R6G).

2.1. Nano-Photocatalyst

As it can be observed in Tables 1–3, the photocatalytic membranes prepared so far were mostly synthesized using semiconductor materials such as TiO_2 [15,16,18,23–26,28,29,36,47,52–60,64,65,68,83,84,86,88,89], ZnO [44,45,48,63,67], g-C_3N_4 [34,40,71], and Fe_2O_3 [75]. Most of them are metal oxides such as TiO_2, ZnO, and Fe_2O_3. Titanium dioxide (TiO_2) is the most commonly used semiconductor for photocatalytic membranes, due to its chemical and thermal stability, low cost, high reusability, and excellent yield in the degradation of organic pollutants. The main disadvantages of TiO_2 are the high electron-hole recombination ratio, and large bandgap (3.2 eV) that implies a low adsorption capacity for visible light [3,90]. To avoid these limitations some strategies such as doping with a co-catalyst are being tested. The introduction of doping agent into the bulk photocatalyst provides a large dipole moment to change the electron transfer kinetic, and more electrons can be transferred from valence band (VB) to conduction band (CB) of the photocatalyst, hence narrowing the E_g value. The low E_g value indicates a better absorption ability in the visible light or natural sunlight. The incorporation of two semiconductors forms a hybrid photocatalyst, where the photo-generated electrons can flow from more negative to less negative fermi energy (E_F) in CB, while holes flow from more positive to less positive E_F in VB at the interface to prevent charge recombination. These new materials have been mostly used in slurry-type reactors and when it comes to photocatalytic membranes inorganic supports [91] or self-standing catalysts [92]. Silver [17,50,69,70,81,85] and iron [30,39,75] are the metals most commonly used, but also palladium [32], cobalt [37,39], and magnetic nickel [42] have been tested. Other elements used are nitrogen [27,32,33,78–80] and boron [39].

Similarly as in suspension systems, in immobilized photocatalysis, the combination of the photocatalyst with other materials is a widely used strategy to enhance their photocatalytic properties and to redshift its bandgap. Composite photocatalysts are synthesized combining the semiconductor photocatalyst with other materials. Many authors have reviewed the use of composites based on TiO_2 in batch suspension systems [3,93], including composites synthesized with carbonaceous materials (GO-TiO_2, rGO-TiO_2, MWCNTs-TiO_2, AC-TiO_2) [94,95] and g-C_3N_4 based photocatalyst (rGO-g-C_3N_4, g-C_3N_4-TiO_2) [96]. Readers are referred to the just mentioned thorough reviews to get deeper insight on the photocatalytic activity of those materials, as it is not the objective pursued with the present review. As Tables 1–3 show, the use of composite materials has been extended to the preparation of photocatalytic membranes. Carbon materials that include graphene oxide (GO) [69,73,74,76,77,79,82], reduced graphene oxide (rGO) [20,33,38,61,70–72,75], activated carbon (AC) [22], carbon nanotubes (CNTs) [35,80], multi-walled carbon nanotubes (MWCNTs) [21,62,85], graphitic carbon nitride (gC_3N_4) [34,40,41,71], and carbon quantum dots (CQDs) [87] have been immobilized in polymeric membranes. Certain carbon materials develop high surface area and in general provide good mechanical properties, together with antimicrobial properties [69].

Additionally to the photocatalytic activity, the introduction of semiconductor nanoparticles in the membrane matrix can also lead to: (i) the enhancement of the membrane hydrophilicity due to the photocatalyst polarity, and (ii) the modification of the membrane morphology during the synthesis. The influence on membrane morphology will be further discussed in the section covering the membrane synthesis methods of the present review. Some authors have observed a so-called superhydrophilicity of polyvinylidene fluoride (PVDF) [15,18,59], polysulfone (PSF) [28,29], polyethersulfone (PES) [97], PES-F-COOH [43], and polyetherimide (PEI) [83] membranes that incorporate TiO_2. Superhydrophilicity is defined as an intrinsic property of TiO_2 surface that generates a significant increase in water flux under UV or sunlight conditions [15,16,59,98]. The mechanism of TiO_2 nanoparticles superhydrophilicity is depicted in Figure 2. As the TiO_2 is UV-irradiated, the photo-generated electrons reduce Ti^{4+} to Ti^{3+}, and the O^{2-} anions are oxidized to O_2 in the photocatalyst holes. Oxygen vacancies are produced on the surface, so the empty sites can be occupied by the water molecules, and OH^- groups are adsorbed on the surface, which increases the surface hydrophilicity [97]. In consequence, the water permeate flux is increased [18,28,29,43]. Composites with ZnO particles also provided improved permeation flux in references [44,45].

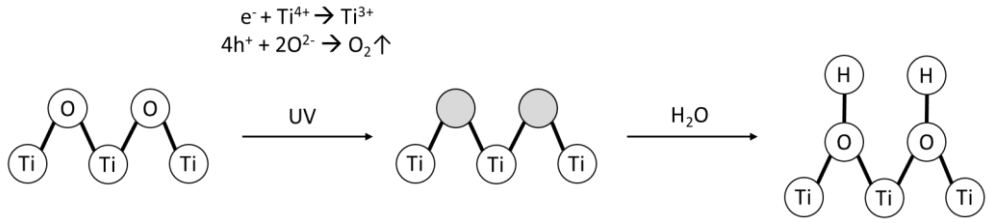

Figure 2. Mechanism of superhydrophilicity. Adapted from [97].

To find out the optimum photocatalyst concentration to be immobilized in a membrane is not trivial. Multiple factors can influence this variable as stated in the revised literature, such as the selection of the photocatalyst and the polymer materials, the synthesis method and the membrane macrostructure, among others. As Tables 1–3 show, a wide variety of photocatalyst concentration ranges has been studied, from 0 wt. % to 30 wt. % for similar systems. Particularly, the synthesis method and the processing variables exert an important influence. Therefore, the critical analysis of the optimal nanoparticle concentration observed by different authors will be addressed in the specific membrane synthesis section.

2.2. Polymer

The selection of the polymer matrix material is a key point in the performance of photocatalytic membranes. As it was already mentioned in the introduction, the support material must be resistant to the degradation caused by UV irradiation and by the generated oxidants. Therefore, this section overviews the different polymers reported in the literature to develop photocatalytic membranes, focusing the attention on their chemical, and particularly, photochemical resistance.

Tables 1–3 show that several polymers have been used to produce photocatalytic membranes. These polymers can be grouped in:

1. Fluorine-based: polyvinylidenefluoride (PVDF), poly(vinylidenefluoride–trifluoroethylene) P(VDF-TrFE), polytetrafluoroethylene (PTFE), and a copolymer of PVDF and hexafluoropropylene (PVDF-HFP)
2. Sulfur-based: polysulfone (PSF), and polyethersulfone (PES)
3. Nitrogen-based: polyacrylonitrile (PAN), polyethylenimine (PEI), polyamide (PA), and polyamide 6 (PA6)
4. Cellulose derivatives: cellulose acetate (CA), and mixed cellulose esters (MCE)
5. Other polymer: polycarbonate (PC)

Among all polymers, PVDF is the most widely employed material for photocatalytic applications in literature, followed by PAN, PES, PSF, and CA. Other polymers such as PTFE, PC, PDA, and MCE are less frequently used. PVDF, P(VDF-TrFE), PTFE, PSF, and PES are hydrophobic polymers while PAN, PEI, CA, MCE, and PC are considered hydrophilic. PVDF, PTFE, PES, PSF, and PAN are polymers usually employed to synthesize mixed matrix membranes because they are easy to process. On the other hand, porous CA, MCE, PC, and PEI membranes are usually employed as supports for thin-film composite photocatalytic membranes.

For mixed-matrix membranes fabrication (Tables 1 and 2), PVDF is the most commonly used polymer [15–18,20–23,25,26,52–60,62,84,86,88] due to the strength and stability of the C-F bond. Other fluorine-based polymers are P(VDF-TrFE) [46] and PVDF-HFP copolymer [50], which presents similar properties than PVDF, and to a lesser extent, PTFE [63,64]. PVDF is commonly used in microfiltration or ultrafiltration membranes as it presents good thermal and chemical resistance [15]. One of the major drawbacks of these fluoropolymers is their high hydrophobicity and therefore low water filtration fluxes. A strategy to improve the wettability of P(VDF-TrFE) membranes was developed by incorporating hydrophilic fillers, such as NaY zeolite type [49].

Sulfonated polymers, i.e., PSF [28–35,51,82] and PES [36–43,69,89] have been widely used to manufacture photocatalytic membranes [28,38]. Both are commercially available polymers with excellent thermal, chemical, and biological stability, good mechanical properties, and high rigidity. However, due to their hydrophobic nature, membranes made with PSF and PES provide low water flux and fouling problems arise, because of the strong interaction between hydrophobic compounds and the membrane surface. Moreover, sulfur-based polymers have poor resistance to UV irradiance [28–30,32,34,38,39,43], as the C-S bond is weak and unstable under UV light and oxidative conditions [99,100].

PAN is a non-toxic polymer and presents UV and chemical resistance [66,80,81]. It is commercially available and environmentally stable. Moreover, it provides good mechanical properties, particularly its flexibility. PEI, whose chemical formula is $(C_{37}H_{24}O_6N_2)n$ [83], PA [85], and PA6 also known as nylon 6 [65] are other nitrogen-containing polymers that have been attempted to a lesser extent for preparation of photocatalytic membranes.

CA and MCE are polymers widely used in the preparation of membranes for water purification and biomedical applications due to their good mechanical strength, water affinity and especially their easy availability and low cost. Among their drawbacks, these materials have low chemical and thermal resistance [44,45]; to overcome these disadvantages, CA is combined with other polymers such as polystyrene (PS) [44], polyurethane (PU) [45], or with nanomaterials such as graphene oxide [79].

Finally, PC [73,74] commercial membranes are mostly used as supports, for the case of thin-film photocatalytic membranes.

The resistance to UV light of several polymeric PAN, CA, PVDF, PTFE, PSF, PES, and PC commercial membranes in the presence of TiO_2 under photocatalytic conditions was studied by Chin et al. [99]. Membranes made of PSF, PES, PC, and CA broke before 30 days of exposure to light irradiance. The rest of the materials were tested again by adding hydrogen peroxide. The authors concluded that PVDF and PTFE showed the highest resistance to oxidative conditions. Meanwhile, PAN membranes reported reduced mechanical properties, leading to the breakup of the PAN membrane. However, there is still an important lack of information about how photocatalytic membranes produced by different processing techniques and polymer materials perform under long-term exposures to UV-light. In the following sections, a specific analysis will be directed to address this issue.

3. Membrane Synthesis Method

The membrane morphology and nanoparticles distribution will depend on the synthesis method employed to incorporate the photocatalyst in the membrane. Below, a thorough analysis of the influence of processing variables on membrane morphology will be performed. The objective pursued is to establish processing guidelines to attain the desired membrane morphology.

3.1. Mixed Matrix Composite Membranes Synthesis Methods

As it is shown in Tables 1 and 2, two different synthesis methods have been reported to immobilize photocatalyst nanoparticles embedded in the polymer matrix: (i) phase inversion and (ii) electrospinning, respectively. For both techniques, the photocatalyst nanoparticles are dispersed in the polymer solution before the membrane synthesis; thus, during precipitation of the polymer photocatalyst nanoparticles remain embedded into the polymer matrix.

3.1.1. Phase Inversion

Phase inversion is the mechanism that takes place in the membrane formation following different polymer coagulation routes such as i.e., Non-solvent Induced Phase Separation (NIPS) or Evaporation Induced Phase Separation (EIPS) [101]. These techniques applied to classical systems of three components can be extrapolated to quaternary systems. These techniques produce two configurations: flat membranes and hollow fibers, that have been reported in the literature as indicated in Table 1. Flat photocatalytic membranes are simple to produce and very useful for laboratory-scale evaluation [101],

and mainly incorporate bare TiO_2 or TiO_2 composites combined with other substances. However, the large surface area provided by hollow fibers might be required to accomplish scalable technologies. Hollow fibers are made by extrusion techniques [52,58,59]. In particular, co-extrusion allows to create two membrane layers with different functional characteristics, the inner part acting as support and the outer part that contains TiO_2 nanoparticles and gives to the membrane photocatalytic and/or antifouling function [52–57].

When the membrane is synthesized by NIPS, a solution formed by a polymer dissolved into an organic solvent and blended with the photocatalytic nanoparticles is forced to demix via its introduction into a bath of a non-solvent, also known as coagulant. At this moment, there is an exchange between the solvent and non-solvent, which must be miscible. The polymer solution separates in two phases at equilibrium, one of them is rich in polymer (solid containing the photocatalyst) and the second one is poor in polymer (liquid). The thermodynamics of this process is explained through the Flory–Huggins theory based on Gibbs free energy equations and interaction parameters of the components. Figure 3 shows an exemplary diagram with the main thermodynamic elements and a typical precipitation pathway of a polymer in NIPS membrane fabrication process. Binodal and spinodal curves are represented in ternary-phase diagrams. As a result of the addition of photocatalytic nanoparticles, such as TiO_2, the diagram of the binodal curve of the ternary system is displaced as depicted in the red line plotted in Figure 3 [102,103]. This will ultimately affect the porous morphology of the polymer membrane and it should be analyzed in detail for each quaternary system.

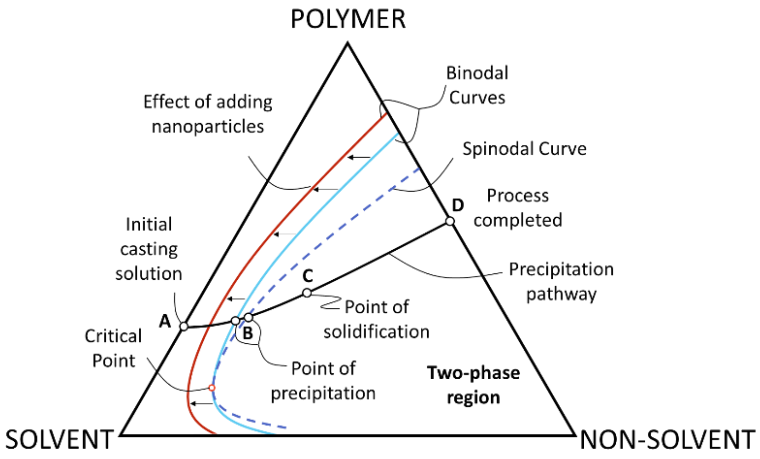

Figure 3. Ternary phase diagram with a precipitation pathway. Adapted from [102].

Additionally, the kinetics of the exchange between the solvent and non-solvent would affect the membrane morphology. When the exchange is fast, the pathway followed by the change in the mixing composition would cross the binodal line earlier; thus, big finger-like pores and asymmetric membrane morphology are expected. Otherwise, when the exchange kinetics is slow, small sponge-like pores are usually obtained.

PVDF and sulphur-based polymers i.e., PSF and PES are the polymers mostly used to develop photocatalytic membranes by NIPS. TiO_2 -based photocatalyst has been introduced to these membranes to remove some model compounds such as dyes (MB, MO), BSA, or humic acid and organic pollutants as bisphenol A or tartrazine.

Regarding the solvent/non-solvent pairs, as can be seen in Table 1, water is the non-solvent most commonly used. Although a large number of solvent and non-solvent combinations are possible, DMAc/water [15–18,20–23,31,38,39,42,52–57,59] and NMP/water [26,28,32–34,37,40,41,51,58] are the most popular pairs in NIPS (Table 1). DMF/water [35,36,43] and TEP/water [25] are also used but to a lower extent. Membranes from ternary systems polymer/solvent/ non-solvent, where the polymer is PVDF, PSF, or PES, the solvent is DMAc, NMP, or DMF and the non-solvent is water, present the

typical porous asymmetric structure formed by a thin dense top layer, supported by a finger-like structure [15,17,18,20–23,28–30,33,34,36–39,43,51], which is characteristic of instantaneous demixing when water is used as coagulant. Moreover, due to the binodal curves of the systems PVDF/DMAc/water, PVDF/NMP/water, and PVDF/DMF/water being very close, similar membrane structures with the three solvents were obtained [104]. The use of a water: isopropanol (70:30) mix as coagulation bath for TiO_2/PES membranes produce a sponge-like structure [19].

Regarding quaternary systems, the most popular photocatalysts dispersed on the polymer solution are TiO_2 and ZnO as shown in Table 1. The photocatalyst concentration affects importantly the rheology of the polymeric solution [15,19,29]. Figure 4 gathers the effects of the photocatalyst concentration on the polymeric solution rheology and the consequent membrane performance. On the one hand, at low concentrations of the photocatalyst, the viscosity of the polymer solution slightly and progressively increases. The hydrophilic groups of the catalyst attract the water molecules that diffuse faster towards the polymer phase, so as previously mentioned, the binodal curve shifts to the left of the ternary phase diagram (see Figure 3). This will ultimately accelerate the demixing rate, producing bigger and distorted finger-like pores and an increase of the membrane porosity. On the other hand, at high concentration of photocatalyst, due to the strong interaction between the photocatalyst nanoparticles and the polymer molecules, the viscosity increases abruptly, the polymer solution changes its nature from Newtonian to non-Newtonian fluid and the membrane formation is governed by the kinetics, that is radically slowed down reducing the pore radius and membrane porosity. This phenomenon is directly related to the membrane performance. At the photocatalyst concentration of the rheological change (Figure 4), the flux, the porosity, the pore size, the hydrophilicity, and the mechanical properties, such as breaking strength, reach a maximum ('optimum') value [15,19,23,26,28–30,36,38,39,43,53,59,61,63] From this point on, the membrane properties, i.e., flux, pore size, porosity, etc., decrease and additionally the photocatalyst nanoparticles tend to aggregate. The nanoparticles aggregation could be avoided if a strong chemical bonding is achieved between the nanoparticles and the polymer chains, for instance, using silane (γ-aminopropyltriethoxysilane) as a coupling agent to form a covalent link between the photocatalyst and the polymer [43].

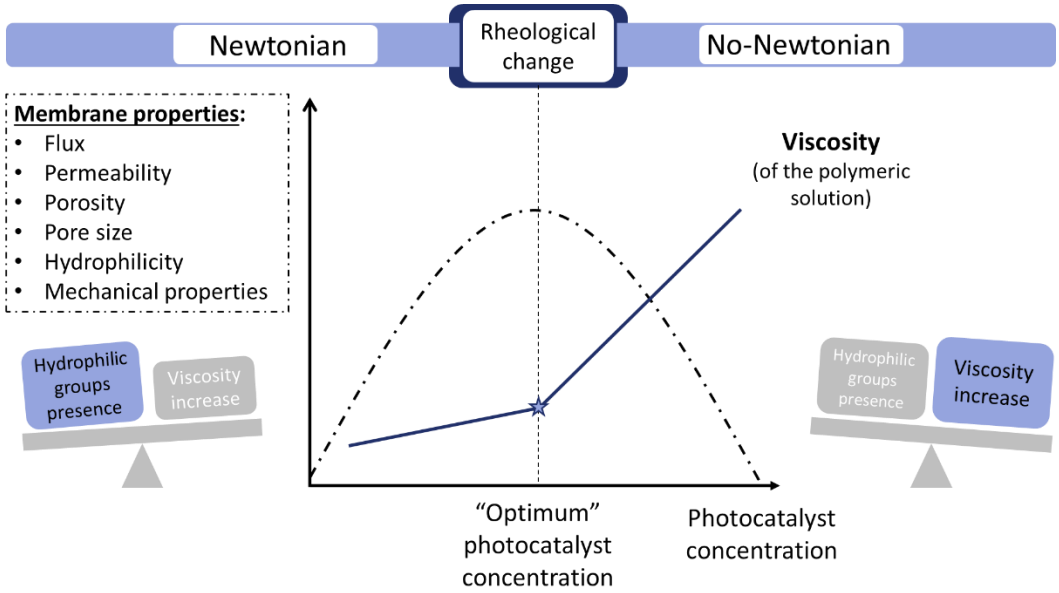

Figure 4. Rheological change of the polymeric solution when the photocatalyst concentration reaches certain value.

Additionally to the photocatalyst, some works incorporate other additives or fillers to the polymer solution [15,17,18,20,21,23,24,30,33,34,38,39,43,51,57–59,62]. Some of these additives are i.e., leachable

agents such as polyvinyl pyrrolidone (PVP) [17,18,20,21,33,34,38,39,43,51,58,59] and polyethylene glycol (PEG) [15,23,30,57] and inorganic salt as lithium chloride (LiCl) [24], which increase the membrane pore size and the number of pores. Surface modifier macromolecules (SMM) are tailormade polymers with tuneable hydrophobicity. As hydrophilic SMMs have lower surface energy than polymers, they migrate to the air/membrane interface to minimize the total free energy of the system. Its addition to the polymer solution forms a denser skin layer and forces the photocatalyst migration to the active layer of the membrane [40,41]. Another interesting strategy to arrange the position of the photocatalyst is the use of magnetic nanoparticles. Sun et al. [42] applied a magnetic field over a casted solution of PES and magnetic Ni-TiO_2 catalyst before the immersion to the bath coagulation. The particles moved to the surface of the membrane instead of being homogeneously dispersed in the membrane matrix, confirmed by Ni and Ti mapping test of SEM images.

Finger-like microstructure usually produces membranes with low mechanical stability. On the other hand, the sponge-like structure would allow the membranes to avoid membrane compaction during filtration. This structure can be obtained with slow polymer precipitation techniques. For instance, in EIPS [101] the polymer precipitation is induced by solvent evaporation, which retards the polymer solidification. A slow precipitation mechanism usually produces membranes with a dense homogeneous structure. However, it has been reported the EIPS synthesis, using DMF as a solvent, of homogeneous sponge-like photocatalytic membranes with controlled porosity and pore size of P(VDF-TrFE) [46–49] and PVDF-HFP [50] copolymers when adding TiO_2 [46–49], Ag-TiO_2 [50], and/or ZnO [48] as photocatalysts.

The sponge-like structure can be also obtained by controlling the solvent evaporation time before the introduction of the polymer solution into the coagulation bath in a NIPS process [25,40,41]. When the solvent (NMP) evaporation time was below 5 min, g-C_3N_4 doped polymer membranes with an asymmetric structure formed by a dense top-layer and finger-like structure sub-layer were obtained. Above this evaporation time, the structure changed from finger-like to sponge-like [40,41]. In other works, using TEP as the solvent with an evaporation time of 2.5 min [25] or using isopropanol: water as the coagulation bath [19], TiO_2 containing polymer membranes presented sponge-like structure.

The variables employed during the phase inversion, such as i.e., components, composition, and solvent evaporation time, importantly affect the ultimate membrane morphology in terms of pore size and pore structure. Figure 5 depicts schematically the different types of variables that mainly influence the membrane structure when phase inversion techniques are used.

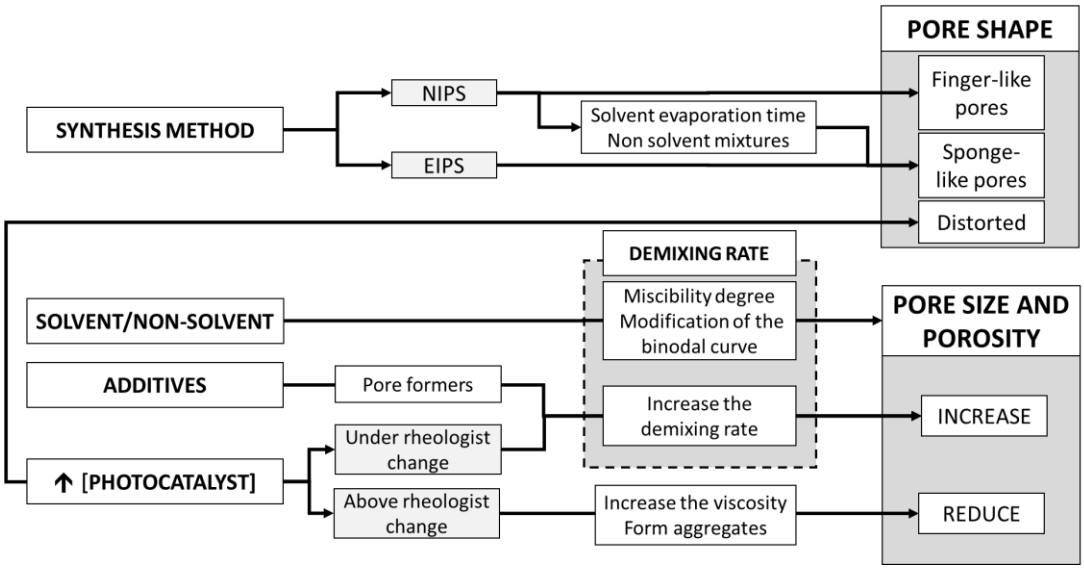

Figure 5. Schematic overview of the influence of phase inversion variables on membrane structure.

3.1.2. Electrospinning

Electrospinning is a simple, versatile, and low-cost way to synthesize polymeric nanofibers [66,80]. A high potential gradient is applied between the grounded collector and the polymer solution droplet. When the electrostatic potential overcomes the polymer solution droplet surface tension, charged threads of the polymer solution are formed with fiber diameters in the order of some hundreds of nanometers [105]. During this processing technique, as it has been revised in Tables 2 and 3, micro/nano-fibers have been usually collected in flat mats. In most cases, photocatalysts such as bare TiO_2 [64,65,68], and ZnO [63,67] or composites as GO-TiO_2 [61], and TiO_2-ZnO [66] were incorporated to the fiber (Table 2). In addition, electrospun mats could be used as supports for TFCM as indicated in Table 3 [75,81,87,88].

The morphological structure of the fibers can be tailored by changing different processing variables, such as the polymer molecular weight, polymer concentration, and flow rate of the polymer solution, tip to collector distance, and applied electric voltage [61,66,67,79,88]. In general, solid (non-porous) polymer fibers are produced. The bulk porosity of the mat is formed by the interstitial separation among the deposited micro/nano-fibers. Electrospinning allows high aspect ratio (length/diameter) of the fibers and uniform diameter, which means large specific surface area [61,80].

As can be seen in Tables 2 and 3, DMF is the principal solvent used [66–68,79,80] and to a lesser extent water [63], DMAc [87] and mixtures of acetic acid: formic acid [65] have been also used.

Regarding the polymer materials usually employed to produce photocatalytic mats by electrospinning, PAN is the most widely used polymer [66–68,75,80,81,87] due to its flexible nature and because it is easy to process. PAN fibers have high mechanical strength and are chemically resistant [66,67,81,87]. Other polymers used, although to a lower extent, are PTFE [63,64], P(VDF-TrFE) [61], PA6 [65], CA [79] and PVDF [86].

The photocatalytic nanoparticles of TiO_2, ZnO, among others (see Table 2) are mostly incorporated and homogeneously dispersed in the polymer solution [61,63–68], and subsequently electrospuned.

The rheological change of the polymer solution caused by the photocatalyst incorporation at high concentrations also causes the agglomeration of the nanoparticles and consequently the formation of beads which could affect the polymer structure [106]. In most cases the fiber diameter and porosity increase with the photocatalyst concentration due to the increase of the solution viscosity [63,65–67], as can be extracted from scanning electron microscopy (SEM) images. When using ZnO concentration higher than 20 wt. %, there is adhesion between the nanofibers. As a result, the mat porosity decreases blocking the light access inside the mat [63]. However, Almeida et al. [61] found that the fiber diameter and porosity decreased with the increase of the TiO_2/GO concentration due to mechanical stretching during the material processing caused by an increase in the solution electrical conductivity when doping GO to form composite TiO_2/GO photocatalyst nanoparticles.

The selection of the polymer material limits the dosage of nano-photocatalysts in the polymer solution. When fibers are synthesized with fluorine polymers it is possible to work with photocatalyst concentration up to 20 wt. % of TiO_2/GO and ZnO [61,63]. Membranes that use PAN usually work with photocatalyst concentration below 2 wt. % including TiO_2-ZnO [66], and ZnO [67].

3.2. Thin Film Composite Synthesis Methods

Table 3 shows different coating techniques to prepare thin-film photocatalytic membranes, including vacuum deposition also called vacuum filtration [69–75], filtration [76,77], immersion [78–85], electrospraying [86], co-electrospinning [87], hot-press deposition [88], and sputtering followed by anodization [89]. Being immersion and vacuum deposition, the techniques mostly used. In this case the main photocatalysts incorporated to the membrane were TiO_2 [83,84,86,88,89] and composites of TiO_2 with carbon based compounds [69,70,72–74,76–80,82], among others (see Table 3).

Commercial microfiltration membranes with a pore size between 0.2–0.45 μm are frequently used as supports to be coated with the photocatalyst [70,71,73,74,76,77,84,85,89]. The use of ultrafiltration membranes is less common [69,78,82]. Commercial supports can be made of different materials as can

be seen in Table 3, but the most used polymer is CA [70,71,76,77]. However, tailor-made supports have also been produced by phase inversion [83,88] or electrospinning [68,75,79–81,86,87].

The photocatalyst loading capacity depends on the synthesis technique. For instance, Table 3 shows that it is possible to successfully coat membranes with a photocatalyst (nAg-GO-TiO_2 [69], Ag-rGO-TiO_2 [70], rGO-g-C_3N_4 [71], and GO-TiO_2 [72]) concentration up to 8 mg/cm^2 when vacuum deposition is used as a synthesis method, being the optimum concentration is around 0.8-2 mg/cm^2. However, when using filtration or immersion deposition of TiO_2 [83], or carbon based photocatalyst [76–78], the working photocatalyst concentration can be increased up to 35 mg/cm^2 and the optimum concentration is in the range 7–20 mg/cm^2.

As Figure 6 shows, different strategies can be followed to anchor the photocatalyst on the membrane surface and then ensuring long-term stability. The most popular technique is the use of an additive to cross-link the photocatalyst and the polymer through physical or chemical interaction. For instance, chemical bonding is achieved with polyallylamine (PAAM) used to link nAg-GO-TiO_2 photocatalysts to PES membrane [69] and glutaraldehyde (GA) to link NH_2-TiO_2 on the one hand to a CA membrane blended with GO [79] and on the other hand to PAN-CNT [80] membranes. This linking was possible because the amino groups of PAAM and NH_2 react with GO and CNT nanoparticles creating C-N bonds. Polyethylene glycol (PEG) and GA to link Ag-rGO-TiO_2 [70], and polyvinyl alcohol (PVA) is used to anchor AC-N-rGO-TiO_2 nanoparticles [78] to commercial polymer membranes of CA and PSF, respectively. Due to the saponification degree of PVA (98–99%), it is demonstrated that the PVA coating is not dissolved during the degradation and filtration process [78]. All of these photocatalysts are TiO_2-based composites with carbonaceous compounds, silver, or amino groups.

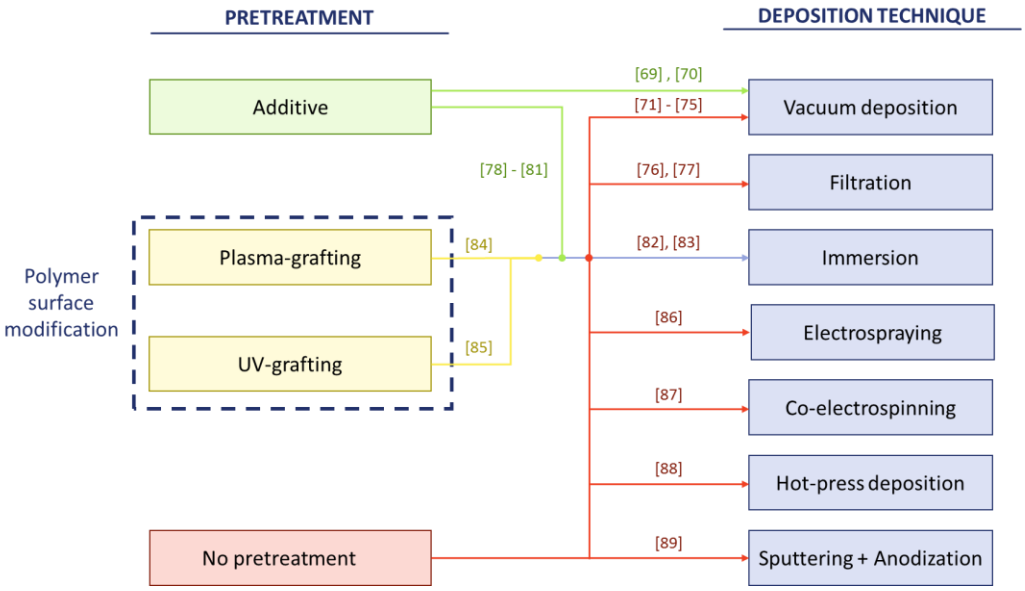

Figure 6. Strategies to ensure the photocatalyst membrane adhesion in thin film composite coating methods.

The in situ synthesis of composite membranes, which has been exhaustively reviewed by Li et al. [107], is another popular approach to improve the long-term stability of the nanoparticles in the membranes. Related to this, only one work analyzed in this review applied in situ deposition, one of them using polydopamine (PDA) as an additive that facilitates the in situ immobilization of Ag-TiO_2 nanoparticles [81]. High temperatures are required for the in situ growth of the photocatalyst in the membrane, so this could be the reason why only one work uses this technique in polymeric membranes.

The surface modification of the polymeric substrate is employed to create binding sites for the photocatalyst or facilitate its adhesion. For instance, plasma-induced graft polymerization is a technique that eliminates the need for a chemical initiator and is followed by immersion. Commercial

PVDF membranes were modified by plasma-grafting which generates activated species that can trigger polymerization reactions [84]. The liquid grafting was made by the introduction of the plasma pre-treated membrane in a polyacrylic acid (PAA) polymer solution. Binding sites were created in the membrane surface that facilitated the self-assembly of TiO_2 nanoparticles as a thin and uniform coating. The number of binding sites was controlled and maximized by the modification of plasma-grafting conditions (plasma treatment: 100 W for 120 s; liquid graft: 70% acrylic acid solution at 60°C for 2 h). Similarly, the grafting can be initiated by UV irradiation [85], in this case the Ag-ZnO-Fe_3O_4-MWCNT/PAA was grafted to a PA membrane support.

More elaborated coating techniques also ensure the good adhesion of the photocatalyst to the support as electro-deposition techniques that includes electrospraying [86] and co-electrospinning [87]. Hot-press is a process in which pressure and temperature are applied to adhere the photocatalyst fibers, by a partial fusion, to a polymeric membrane surface; the field emission scanning electron microscopy (FESEM) cross-section images indicate a great adhesion between TiO_2 as photocatalyst and PVDF as the membrane matrix [88]. Sputtering is a physic process where there is vaporization of Ti atoms from a solid material "blank" by bombarding it with energetic ions then, by anodization, Ti atoms crystalize forming TiO_2 nanotubes which are firmly bonded to the PES commercial support [89].

However, in the cited literature, most of the works [71–77,82,83] do not use any additive or additional technique to ensure the photocatalyst attachment. To further analyze the photocatalyst stability, chemical evidences of the particle leaching from the membrane should be followed during the experimental evaluation of the membrane performance. Works complying this study are analyzed in the sections below.

4. Membrane Functionality

The incorporation of photocatalytic nanomaterials can lead to the following functional improvements in polymeric membranes: (1) membranes with antifouling properties and the consequently improved filtration capacity and reusability, (2) membranes with photocatalytic activity, or (3) a combination of the above two functional features. Below, a detailed analysis of the filtration and photocatalytic properties of the reported membranes will be addressed in terms of the influence of the membrane synthesis method. Additionally, general guidelines about the processing variables advisable to achieve improved membrane performance and membrane long-term stability will be emphasized.

4.1. Filtration Performance

Membranes intended for filtration applications were made by NIPS and EIPS in the case of MMM, while both commercial polymeric supports and NIPS-homemade supports were employed for TFCM. The functionality of MMM and TFCM membranes was analyzed in terms of hydraulic permeability and antifouling properties and compared to neat polymeric membranes. The hydrophilic enhancement provided by TiO_2 automatically benefited the permeability and antifouling properties of TiO_2-functionalized membranes [21,22,38], without the necessity of applying further UV irradiation (and therefore additional photocatalytic action). In other cases, the organic deposits on the functional membranes were cleaned by photocatalytic degradation after membrane filtration [17,23,43] using cycles of membrane filtration-UV irradiation cleaning. Below a detailed analysis of the membrane features and their influence on the hydraulic permeability and antifouling effect of the modified membranes will be addressed.

4.1.1. Hydraulic Permeability

The effect of adding TiO_2, AC, GO, and TiO_2 carbon-based nanomaterials on the structure and filtration properties of PVDF and PSF membranes, prepared by NIPS are shown in Table 4.

Table 4. Permeability, pore size, and porosity comparison between neat and composite membrane.

Neat Membrane				Composite Membrane				
Polymer (%)	**Permeability (L/hm^2bar)**	**Mean Pore Size (nm)**	**Porosity (%)**	**Nanoparticles Added (%)**	**Permeability (L/hm^2bar)**	**Mean Pore Size (nm)**	**Porosity (%)**	**Literature**
PVDF (15)	150	48.1	69.6	TiO_2 (1)	300	52.6	75.1	[20]
				GO (1)	400	55.7	78.3	
				GO-TiO_2 (1)	490	65.2	83.1	
PVDF (14)	90	18.6	47.2	AC (0.5)	170	18	56	[22]
				TiO_2 (0.1)	280	28.2	54.3	
				AC-TiO_2 (0.5:0.1)	255	30.6	55.4	
PSF (18)	115	56.2	62.5	GO (0.5)	150	61.4	69.4	[33]
				TiO_2 (0.5)	155	62.8	71.6	
				rGO-TiO_2 (0.5)	180	67.9	77.2	
				N-rGO-TiO_2 (0.5)	230	70.5	81.8	

In Table 4, the values of permeability are directly related with the pore size of the membrane, which is defined by the initial system polymer/solvent/additive. The higher values of pore size reported in Table 4 [20,33] are due to the use of pore formers during membrane synthesis. It can be seen that, as previously indicated, the incorporation of TiO_2 increased the membrane permeability. In the MMMs the increase of membrane permeability could be mainly attributed to the increase of the pore size and the porosity produced by the inclusion of the nanomaterials on the ternary system. The use of TiO_2 modified with carbon-based nanomaterials even enlarged membrane pore size and porosity and therefore higher permeability was attained. As it was previously explained in Section 3.1.1., for MMM synthesized by NIPS, the optimal selection of photocatalyst concentration and its effect on the rheological properties of the polymer solution resulted in obtaining membranes with adequate porosity and morphology. Above the nanoparticles optimal concentration, they tend to aggregate, and it has detrimental effects in the membrane permeability and hydrophilicity. For example, the permeability for a bare PES membrane was found to be 1.1 L/m^2hbar [38]. The addition of nanoparticles increased the pore size, the porosity, and the hydrophilicity (measured by contact angle), thus the permeability improved to 2.25 L/m^2hbar, corresponding to a 1 wt. % of nanoparticles. Above this nanoparticle concentration, the aggregates clogged the pores of the membrane, which increased the water transport resistance of the membrane surface [59] hence, the permeability decreased.

The works that analyze the optimum concentration of TiO_2 [15,19,26,28,29,59] and Fe-TiO_2 [30] conclude that the optimum nanoparticles concentration in the polymeric solution will be between 2–5 wt. % according to the concentration before the rheological change (see Figure 4 and Section 3.1.1), which gives the highest permeability value. This range usually corresponded to a 0.2–0.5 wt. $\%/cm^2$. However, the optimum value should be experimentally found for each system as it will depend on the particular rheological properties of the polymer solution that incorporate the photocatalyst.

Additionally, Tran et al. [16] showed an efficient way to maximize pure water flux, in absence of pollutants, with fewer energy consumption using irradiation cycles of non-UV and UV periods for TiO_2/PVDF flat membranes.

In TFCM, the incorporation of an additional thin layer with low-size pore to a microfiltration or ultrafiltration support typically increases the resistance to the mass transport and even reduces further the support membrane pore size, therefore the flux is reduced [69–74,76,77,82,89]. This effect has been frequently observed when vacuum [69–74], filtration [76,77], immersion through layer by layer [82], and sputtering [89] deposition were used, using mostly GO-TiO_2 as the catalyst, but also rGO-g-C_3N_4, and TiO_2, see Table 3. On the contrary, three works reported an increase in the membrane flux after the photocatalyst deposition. Nor et al. [88] used the hot-press technique, under controlled temperature conditions (160 °C), to partially melt the TiO_2 photocatalyst to the PVDF membrane. In that case, the porosity of the support remained unaltered and the use of hydrophilic TiO_2 as photocatalyst increased the flux in contrast to the plain support. On the other hand, the flux enhancement is also achieved modifying the membrane support hydrophilicity through two ways, using the hydrophilic PVA as a crosslinker between the AC-N-rGO-TiO_2 coating and the PSF membrane support prepared by immersion [78] or using plasma grafting, which modifies the hydrophilicity of the PVDF support combined with the immersion in a TiO_2 solution [84].

4.1.2. Antifouling Properties

The antifouling behavior has been studied for MMM systems synthesized by phase inversion [15,20–23,26,33,36,38,43,53,57] and for TFCM systems synthesized by vacuum deposition [70,71] and immersion [83–85]. Model organic foulant solutions, i.e., bovine serum albumin (BSA) protein [15,17,20–22,26,84], humic acid (HA) [23,36], and polyacrylamide (PAM) [43] are usually employed for studying antifouling phenomena.

The benefits of immobilizing photocatalysts for the membrane antifouling property can be associated with: (i) an increase of the hydrophilicity and (ii) a decrease of the membrane roughness. As it has been previously explained, the use of bare TiO_2 produced an enhancement of the

hydrophilicity [15,23,24,36,43,53,57,83,84], which can be enhanced even more when the material is irradiated with UV light. In addition, this property might be intensified when carbon based composite photocatalysts are used [20–22,33,38,70,71] considering the synergy between carbon compounds and TiO_2 [20]. This synergy is produced because the presence of oxygen-containing functional groups (hydroxyl, epoxy, carboxyl, and carbonyl) in the surface of the photocatalyst facilitates the interaction of carbonaceous materials with a wide variety of organic and inorganic materials that helps avoiding the aggregation of the nanoparticles [72,75]. Furthermore, in MMM the use of additives, i.e., PEG [57], also improved the anti-fouling property because this additive generated smoother membrane surface.

As it was previously mentioned for MMM, at the photocatalyst concentration of rheological change, the permeability, the porosity, the pore size, and the hydrophilicity of the membrane reach a maximum [15,26,36]. In most of the cases, this concentration matches with the one that gives the best antifouling performance [15,29]. The best antifouling performance occurs at the concentration where the flux recovery ratio is the highest and the irreversible fouling is the lowest.

4.2. Photocatalytic Activity

4.2.1. Comparison between Suspended and Membrane Immobilized Systems

In general, it has been reported that the SPMRs permit to achieve higher degradation yields of POPs when compared to IPMRs, due to the larger active surface area, which guarantees a good contact between the photocatalysts and the pollutants. As a consequence, there are more studies of SPMRs. However, fouling, which is caused by deposition of the photocatalyst nanoparticles on the membrane surface with a consequent flux decline, and light scattering, still limit the performance of this type of PMRs configuration [4,108,109]. Meanwhile, in the IPMRs, the photocatalyst/pollutants contact is hindered by the mass transfer limitation over the immobilized photocatalyst. However, in this configuration, catalyst recovery and reuse can be more easily achieved than in SPMR and it is potentially less hazardous.

In general, few works have been found in the literature comparing the photocatalytic activity of (i) systems with immobilized photocatalyst, and (ii) the corresponding amount of suspended photocatalyst. In terms of membrane functionality, this comparison is a key point. It will help to determine the synthesis method that preserves the photocatalyst activity once it is immobilized or improve the dispersibility of the immobilized photocatalyst; the latter will favor enhanced performance when compared to suspended systems. When MMMs are used, a slight reduction of the photocatalytic performance compared with suspended systems has been so far observed. This reduction, in most of these works, can be considered inside the experimental error (<5–10%). For instance, flat membranes made by EIPS showed a negligible reduction in the photocatalytic degradation yield of MB of 3% using TiO_2-NaY/P(VDF-TrFE) [49]; in the case of NIPS membranes, the photocatalyst performance decayed down to 6% (Co-TiO_2/PES) [37] and 15% (O-g-C_3N_4/PES) [41] for the degradation of 2,4 dichlorophenol and phenol, respectively. For electrospun nanofibers, using TiO_2-MWCNTs/PVDF nanofibers to degrade MB, the performance loss was 12% compared to the suspended photocatalyst [62]. Finally, degrading MO with ZnO/PAN nanofiber mat, the efficiency loss was about 4%, which means that the nanofiber photo-activity is 1.6 times less than the photocatalyst (ZnO) powder [67]. As it can be seen, in general low performance reductions on immobilized photocatalysts on MMMs were always reported (<15%) compared to suspended systems

However, Ramasundaram et al. [86] showed an interesting comparison of the photocatalytic activity between TiO_2 (i) in suspension, (ii) deposited by electro-spraying on PVDF nanofibers mat (TFCM), and (iii) immobilized in PVDF MMM by NIPS; these authors analyzed different synthesis methods. Total degradation of MB and IC was achieved with TiO_2 suspension in 40 min, while for the electrosprayed nanofibers mat, the time to achieve the degradation increased up to 60 and 100 min for each pollutant respectively. Furthermore, after 140 min of irradiation, the pollutants studied were not completely degraded with the MMMs. From these results, a lower photoactivity of MMM is observed,

attributed to a lower photocatalyst active surface area in contact with the pollutant, in contrast to the suspended system.

Overall, attending to the aforementioned results, it could be that the dispersibility on the polymer matrix of MMMs of bare TiO_2 might be more difficult than for other photocatalysts, such as composite TiO_2 photocatalyst or other type of semiconductors. However, more detailed studies should be done to confirm this preliminary observation.

4.2.2. Influence of the Synthesis Method on the Membrane Photocatalytic Performance

As previously remarked, it has been observed in the literature that the different photocatalyst immobilization methods resulted in different photocatalytic performances. This effectiveness might be attributed to different photocatalyst accessibility to light sources. Therefore, the in-depth analysis of the effect of the method of membrane synthesis on the allocation of the photocatalyst in the membrane matrix is; this analysis is focused to evaluate the potential relationship between the photocatalyst entrapment or shielding effect within the membrane and its photocatalytic activity, as well as its long-term stability.

In the case of phase inversion MMMs, the nanoparticles could be homogeneously dispersed in the whole membrane matrix, so they could be embedded in the membrane and therefore the number of nanoparticles accessible to light could be importantly reduced. To overcome this problem, dual-layer hollow fibers provide an external photocatalytic layer, while the inner layer is not photocatalytic. Within this strategy, similarly than in TFCM strategies, the filtrating performance of the membrane might be hampered with the additional photocatalytic layer. Therefore, it is often necessary to reach a compromise on the photocatalyst concentration and be careful with the pore structure of the coating layer. Different works have observed that the best photocatalytic performance of double layered TiO_2/PVDF hollow fibers [56] and flat membranes of TiO_2/P(VDF-TrFE) prepared by EIPS by Teixeira et al. [48] was achieved with a 15 wt. % of photocatalyst concentration. Further concentration increase would limit the photocatalytic activity due to the nanoparticles agglomeration with the consequent decrease the surface area. However, regarding the filtration performance of the double layered TiO_2/PVDF hollow fibers, Dzinun et al. [53] observed that at a concentration of 3 wt. % of TiO_2 the highest membrane flux was achieved as further concentration of photocatalyst blocked the membrane pores. Overall, Dzinun et al. [49] observed that a concentration of 3 wt. % of TiO_2 could be considered adequate to perform simultaneous filtration and photocatalytic degradation of NP.

Usually, the electrospun MMMs have been only used to immobilize the photocatalyst and never with filtration purposes as they usually have large macro-pores and therefore, low pollutant rejection. The mat is submerged in the polluted solution and, after the degradation process, it is easily recovered [61,63–68,87]. Similarly as in blended MMMs by NIPS, in electrospun membranes, the photocatalytic nanoparticles, such as ZnO and TiO_2, were homogeneously located in the membrane matrix [63,65]. On the other hand, the nanoparticles of the CQDs-Bi_{20}-TiO_{32} photocatalyst could be also anchored on the surface of the electrospun nanofiber using co-electrospinning [87]. Salazar et al. [50] compared the photocatalytic performance of Ag-TiO_2/PVDF-HFP membranes prepared by solvent casting and electrospinning. Solvent casting membranes present higher degradation rates of norfloxacin (64%) than the nanofibers (51%).

Only 2 out of the 21 works dealing with photocatalytic TFCMs study the influence of the photocatalyst concentration in the degradation of some dyes. On the other hand, most of the works of TFCMs select the optimum photocatalyst concentration based on the point of highest flux, but not based on results of the membrane photocatalytic activity. For instance, for GO-TiO_2/CA membranes prepared by filtration the catalyst concentration that provided the highest permeation flux was 6.85 mg/cm^2 but the best photocatalytic performance to degrade CR was achieved with 27.4 mg/cm^2 [76]. Similarly, for AC-N-rGO-TiO_2/PSF membranes prepared by immersion the optimum photocatalyst concentration was fixed in 6.92 mg/cm^2, although the higher degradation of MO was achieved with 9.22 mg/cm^2 [78]. Most of works in the literature of TFCM synthesis applied the criteria of the highest filtration performance

to set the optimum photocatalyst concentration highlighting the importance of this property on the overall photocatalytic system.

On the other hand, the method of deposition of the thin photocatalytic film on the membranes is of utmost importance on the efficient anchorage of the photocatalyst on the membrane surface. While using vacuum deposition on CA membranes, low photocatalyst concentration could be deposited, i.e., 0.796 mg/cm^2 of Ag-rGO-TiO_2 [70] and 1.99 mg/cm^2 of rGO-g-C_3N_4 [71], with filtration and immersion as synthesis techniques, higher concentration of photocatalyst was attained, 16.75 mg/cm^2 (GO-TiO_2/CA) and 13.95 mg/cm^2 (Ag_3PO_4/PAN). Consequently, lower photocatalytic degradations were achieved with the vacuum deposited TFCMs, however, attention should be paid to the different type of photocatalysts that were used in the works reported above.

The comparison between the photocatalytic performance of TFCM and MMM membranes has been scarcely reported. Wu et al. [78] prepared TFCM with a PSF commercial support coated with a PVA solution to immobilize the nanoparticles (AC-N-rGO-TiO_2) by a surface deposition method. The MMM was synthesized by NIPS, a solution of PSF, PVP, and AC-N-rGO-TiO_2 was prepared in NMP using water as coagulation bath. TFCM presented higher photocatalytic performance (95.2%) than MMM (31.1%). In addition, Ramasundaram et al. [86] compared TFCM with MMM. They deposited TiO_2 by electro-spraying on PVDF nanofibers mat and immobilized TiO_2 in PVDF MMM by NIPS. Surface deposition by electrospraying was more favorable than NIPS to maintain the photocatalyst accessibility to light. In the latter works, the lower photocatalytic performance of the MMM was explained because the blending method encapsulated the nanoparticles into the membrane matrix, which protects the nanoparticles but hinders light irradiation. However, as previously analyzed in Section 4.2.1, many works also reported similar photoactivity of photocatalytic MMMs than suspended systems. Therefore, more attention to the methodology of MMM membranes preparation should be paid; further works comparing the structural features and functional performance of photocatalytic TFCMs and MMMs should be done discerning the advantages and disadvantages offered by the two membrane types.

4.2.3. Membrane Aging

Polymer Stability

Certain polymers are materials susceptible to photolytic and photocatalytic degradation. As photocatalytic membranes are going to be exposed to UV irradiation, membrane aging, and long-term resistance are crucial to their application. It must be remarked that only few works have explored this long-term membrane behavior.

As in MMMs, the photocatalyst is embedded inside the matrix, and there is no additional protective layer over the membrane, the polymer is highly exposed to light effects. In terms of membrane aging, PVDF membranes have demonstrated stability against photocatalytic reaction and UV irradiation in long-term operation [53–55]. After 30 days of UV irradiation, the membranes upheld their integrity despite many cracks were formed on the surface, which increased the membrane roughness, analyzed with atomic force microscopy (AFM). FTIR tests showed a change of the PVDF crystalline phase, besides the formation of –CF=CH- double bond by dehydrofluorination. The dehydrofluorination reaction of PVDF is presented in Figure 7, following the pathway of carbocation reaction using H_2O as a polar solvent and UV as the heat source, described by Dzinun et al. [54]. There was a slight decrease in tensile strength that increased with the increase of the UV exposure time, causing negative impact on the overall stability. SEM images of an mpg-C_3N_4-TiO_2/PSF membrane [34] showed that the membrane structure was maintained without changes after its exposure to simultaneous photocatalytic degradation and filtration of the antibiotic sulfamethoxazole (SMX) during 30 h. Some loss in tensile strength was observed, although the membrane integrity and flexibility were maintained. In the case of MMM synthesized by electrospinning, ZnO/PTFE nanofibers, they only lost 3.8% of mechanical strength after 5 cycles of operation (25 h) [63].

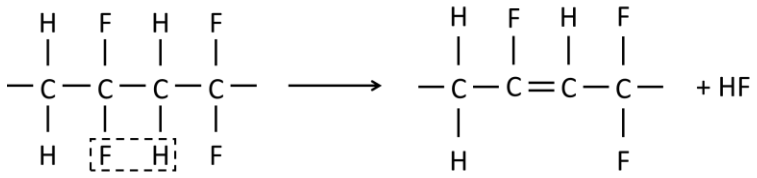

Figure 7. Dehydrofluorination reaction of PVDF through a carbocation reaction where H_2O acts as a polar solvent and UV light as the heat. Adapted from [54].

On the other hand, the TFCM configuration might incorporate a photolytic protective layer to low UV-resistant polymeric supports such as PP [99]. This solution was also pointed out by Tsehaye et al. [100] in their study of the PES membrane stability under oxidative conditions.

Photocatalyst Detachment or Leaching

During operation, photocatalytic membranes might suffer the loss or leaching of photocatalytic nanomaterials. The methodology employed to synthesize the membranes might induce different nanomaterials anchorage on the polymer matrix. However, only two authors evaluate the amount of photocatalyst that leached out from the membrane after each cycle using inductively coupled plasma (ICP). Ramasundaram [86] did not detect any titanium in solution after 10 cycles (17.7 h) of use of a TFCM of electrosprayed TiO_2 on a PVDF nanofibers mat and they observed that the photo-activity was preserved during all cycles. Tissera et al. [67] analyzed the Zn leached from a MMM made of electrospun ZnO/PAN nanofiber after 3 cycles (30 h). Concentrations of Zn of 40, 20, and 17 ppb (which accounted respectively by 0.08, 0.04 and 0.034 μg of ZnO leached per mg of membrane) were measured in the feed tank solution during the first, second and third degradation cycles, respectively. This meant than less than 0.0052% of the photocatalyst embedded in the membrane matrix was leached out of the membrane after 30 h of use.4.2.3.3. Long term membrane performance

Table 5 compiles the works that reused the membrane in several cycles and the change in the degradation rate of organic pollutants. Only 2 out of 5 works of TFCM found a loss of 10% in photocatalytic activity during the cycles of photocatalyst reuse while the others reported stable membrane photocatalytic activity. Meanwhile 6 out of 12 works of MMMs presented a decline in the photocatalytic activity with membrane reuse between 8 and 45% independently of the synthesis method. This means that, similarly, approximately 40% of both TFCM and MMM works report a decline in photocatalytic activity during the reuse of the photocatalytic membranes, although the loss of activity could be more pronounced in the case of MMMs due to the protective effect that the photocatalytic layer could exert on the polymer substrate. Bare TiO_2 or ZnO were used in most membranes collected in Table 5.

Table 5. Influence of the synthesis method on the nanoparticles stability based on the degradation change of the membrane after its reuse.

Photocatalyst/ Polymer	Synthesis Method	Targeted Pollutant	Number of Cycles	Total Irradiation Time (h)	Loss in Degradation Rate (Cycle 1–Last Cycle)	Power of the Lamp	Ref.
MMM							
TiO_2/ PSF	NIPS	Cr (VI)	4	-	0%	Sunlight	[28]
N-TiO_2/ PMAA-g-PVDF/PAN	NIPS	Bentanzon	3	10	0%	UV (5063 lux)	[27]
ZnO/ CA-PS	NIPS	CR, RY 105	5	5	45 %	Sunlight	[44]
TiO_2/ PSF	NIPS	MB, MO	5	7.5	0%	UV-C 10 W	[51]
TiO_2/ P(VDF-TrFE)	EIPS	MB, CIP, IBP	4	20	0%	UV-A 48 W	[46]
TiO_2 or ZnO/ P(VDF-TrFE)	EIPS	MB, Model organic	3	15	13 %	UV-A 48 W	[48]
Ag-TiO_2/ PVDF-HFP	EIPS	NOR	3	15	15.6 %	UV-A 8 W	[50]
Ag-TiO_2/ PVDF-HFP	Electrospinnin	NOR	3	15	8.8 %	UV-A 8 W	[50]
ZnO/ PAN	Electrospinning	MO	3	30	0%	UV-A 40 W UV-B 20 W	[67]
ZnO/ PTFE:PVA	Electrospinning	RhB	5	25	20 %	UV 500 W	[63]
TiO_2/ PTFE	Electrospinning	MB	5	7.5	45 %	UV 300 W	[64]
TiO_2/ PA6	Electrospinning	RBB	3	12	0%	UV 6 W	[65]
TFCM							
TiO_2/ PVDF	Electrospraying	BPA, 4-CP, CMT	10	16.7	0%	4 W	[86]
GO-TiO_2/ CA	Filtration	CR	3	-	10 %	No data	[76]
TiO_2/ PEI-P25	Immersion	RhB	6	12	10%	UV 18 W	[83]
NH_2-TiO_2/ PAN-CNT	Immersion	Cr (VI)	5	5	0%	125 W (420 nm)	[80]
rGO-α-Fe_2O_3/ PAN	Vacuum deposition	MB, MO, RhB, R6G, MG, GV	5	4.2	<10%	UV-vis 275 W	[75]

For instance, in TiO_2/P(VDF-TrFE) MMMs synthesized by NIPS, the degradation rate of MB and the kinetic constants of three consecutive cycles of 5 h each were reported [48]. Particularly, when the membrane incorporated a TiO_2 concentration in the polymer solution of 5, 10, and 15 wt. %, the reduction in the degradation rate between cycle 1 and cycle 3 was 6%, 16%, and 13%, respectively. In this work, nanoparticles were located mainly on the membrane surface and weakly bonded to the polymer, so the authors attributed this effect to the nanoparticles leaching out of the membrane.

It is worth remarking that the important 45% decay in photocatalytic activity reported in Table 5 for some MMMs could be attributed to an important membrane degradation during operation caused by the low chemical and photochemical stability of CA polymer [41] and the high power of the light source employed [60].

Overall, the characterization of the membranes before and after a long-term exposure to UV would help to better analyze membrane aging. The morphological characterization should be done with SEM or FESEM, to obtain images of the membrane surface [55] and AFM, to analyze changes in the membrane surface roughness [54,55]. Additionally, other chemical analytical techniques can be used, X-ray diffractive dispersion (XRD) to observe changes in the crystallinity of the materials employed and energy dispersive X-ray (EDX) to observe changes in the chemical structure of the membrane. Finally, analysis of the functionality of the photocatalytic membrane with filtration tests and photocatalytic reuse tests through ICP analysis of the liquid medium would complete the photocatalytic membrane stability characterization

5. Guidelines and Recommendations for Researchers

This review aims to evaluate the materials, synthesis methods, and their relationship with the functional performance of photocatalytic polymeric membranes. PVDF is the recommended material to fabricate flat or hollow fiber MMMs by phase inversion techniques due to its photocatalytic resistance; this is supported by the large information gathered in the reported works that use this polymer. However, the use of PES and PSF is also popular due to their easy manufacture. In the case of nanofibers made by electrospinning, PAN is the polymer mostly used because it is easy to process by this technique, albeit it is not the most stable polymer under UV-light exposure. On the other hand, in TFCM it seems that the photocatalytic coating generates a protective layer, so supporting materials with low photocatalytic resistance, such as PES or PSF, could be used.

Many works use TiO_2 as photocatalyst for photocatalytic membranes, however, it has been demonstrated that carbon based composite photocatalysts not only improve the photocatalytic performance in both MMMs and TFCMs but also contribute to enhancing between 2 and 3.26 times the filtration performance of the membrane. Moreover, from preliminary observations in this review, it could be stated that TiO_2-based composite photocatalysts could be better anchored and dispersed by linkers on TFCMs than bare TiO_2 nanoparticles.

After an exhaustive review of the synthesis methods for photocatalytic polymeric membranes, not enough evidence was found to select the best methodology and the choice should ultimately be based on the aimed application of the material. The few works that compare the photocatalytic performance of MMM and TFCM have observed that TFCM provided higher photocatalyst surface area of contact with the pollutant, so the degradation is favored with respect to MMM. Nevertheless, in MMM some researchers investigate the synthesis of dual-layer hollow fibers. In this case, the outer layer would have photocatalytic properties and the inner one would act as support to give mechanical strength to the membrane.

Photocatalyst leaching out of the membrane is an important issue. Higher stability of the photocatalyst entrapped in the MMM than in TFCM is expected. However, the use of photochemically non-stable polymers and/or very high powerful light sources could cause the polymer membrane degradation in MMMs and the consequent release of the photocatalyst. Furthermore, in TFCM the use of additives and the application of modification techniques such as surface oximation and plasma-grafting

improves the photocatalyst adherence. Furthermore, no reliable evidence has been found to demonstrate any direct photocatalyst loss attributed exclusively to the membrane synthesis technique.

Finally, although ideally, a good method of photocatalyst immobilization on a membrane could reduce the aggregation of suspended systems, it has been well established in a variety of studies that the photocatalytic degradation activity is normally reduced when the photocatalyst is immobilized in a membrane due to the reduction of the available contact area. This reduction has been studied and quantified in several works giving a range of 3–30%. Therefore, the challenge still persists on the search for a membrane synthesis method that helps reducing nanoparticles aggregation and maximize the area of the photocatalyst exposed to the light source. Herein some guidelines are proposed to help authors in decision-making on the synthesis methodology to produce a membrane with the best performance depending on the required function.

- If a membrane with high filtration and antifouling performance is sought, MMM synthesized by phase inversion is recommended, and particular attention should be paid to the solution rheology to obtain maximum porosity and permeability. The photocatalyst concentration when the rheological change of the polymer solution occurs should be found in the range of 0.2–0.5 wt. % for MMM, albeit each system should be studied in detail. Furthermore, TiO_2-based composites of metal or carbon based materials are recommended.
- If high pollutant rejection is desired, either MMM can be produced with techniques to slow down phase inversion or TFCM techniques, as these would reduce the mean pore size and surface porosity. Among TFCM deposition techniques, vacuum filtration is the least recommended method as it produces the lowest performance in the deposition of the photocatalyst and the least photocatalytic activities.

Based on this literature review, we consider that there are important methodological aspects that should be considered and/or studied more in depth to facilitate future comparison among photocatalytic membranes. Some recommendations can be suggested:

- The influence of the lamp irradiance is crucial on photocatalytic membrane systems, in particular on the effects on membrane aging. In the case of photocatalytic membranes, UV light sources of low power (less than 50 W) or light-emitting diodes (LEDs) are highly recommended to reduce polymer aging and thus, ensuring long-term stability of the membrane.
- Long-term stability is a key issue for process scalability. Therefore, high attention should be paid on this aspect during the membrane viability study. Performing (i) long-term experiments to verify that the membrane maintains its integrity under the experimental conditions, and (ii) reuse experiments to ensure good stability of the photocatalyst is therefore encouraged. It should be considered the effect of elevated heat, UV irradiation and moisture which can lead to polymer degradation.
- The use of analytical techniques such as EDX, XRD, AFM, and SEM or FESEM, before and after the UV exposure, are highly recommended to analyze the aging of the membrane. The quantification of the leaching of nanoparticles from the membrane to the medium should be analyzed with ICP.
- High efforts are being adopted on synthesizing novel and more active photocatalysts. Their physico-chemical characteristics can be notably different from conventional semiconductors such as commercial TiO_2. Nanoparticle dispersions in polymeric matrix present different rheology so the membrane processing can suffer significant changes. These changes could play a key role on the improvement of nanoparticles dispersibility on the polymer matrix so far encountered on MMMs.
- When the membrane has a simultaneous filtration and photocatalytic function, experimental reactors should integrate both filtration and photocatalytic degradation. Membrane functionality characterization should consider: (i) pure water flux test to obtain permeability values (L/hm^2bar); (ii) photocatalytic degradation comparison with the suspended system to evaluate the change in

the photocatalytic activity when the nanoparticles are immobilized, and (iii) pollutant rejection under dark and UV irradiation conditions.

- In the particular case of TFCM synthesis, the influence of the photocatalyst concentration using different coating techniques has not been sufficiently evaluated. There is expected to be an optimal concentration to maintain the balance between the membranes photocatalytic and filtration functions. While, as aforementioned, in MMMs the recommended concentration range is 0.2–0.5 wt. %, in TFMC this evaluation has not yet been assessed and should also be addressed.
- It is noteworthy that most of the works studied in this review analyze the photocatalytic activity using dyes as model organic pollutants. These types of molecules are photosensitive and can be adsorbed on the catalysts and/or on the membranes leading to results that are not representative of other pollutants. Therefore, it is advisable to select other types of organic model compounds, such as, acetic acid, or certain non-biologically degradable organic compounds as those contained in hospital effluents, such as antibiotics, (cautiously) organohalogens, etc., to generalize the obtained conclusions. In this regard, considering the important presence of persistent compounds, antibiotics and disinfectants likely causing bacterial inhibition in the on-site hospital wastewater treatment, the use of photocatalytic membrane reactors for the on-site treatment of hospital wastewaters is envisaged as a promising alternative.

Finally, here we would like to remark that for instance regarding the membrane nature, most PMRs make use of polymeric membranes either in SPMR or IPMR configuration. Although ceramic membranes are less common, their positive characteristics such as high permeability, superior chemical, mechanical, and thermal resistance than polymeric membranes, resistance to UV irradiation, long life, and excellent antifouling properties counterbalance their higher price and there is an expanding trend of applications to wastewater remediation [110].

Overall, the development of fouling resistant and more photo-catalytically active membranes that could maximize the energy adsorbed from the visible light wavelength, together with a deeper knowledge and control of mass transfer limitations in advanced configurations of PMRs and the continuous research of motivating applications will facilitate process design and scale-up, thus, paving the way to establish PMR as one of the best available technologies (BAT) for remediation of wastewaters containing persistent organic pollutants.

Author Contributions: Conceptualization, N.D. and A.U.; methodology, M.R., N.D., and A.U.; investigation, M.R.; writing—original draft preparation, M.R.; writing—review and editing, N.D., A.U., M.J.R., and I.O.; supervision, N.D. and A.U.; funding acquisition, A.U. and N.D. All authors have read and agreed to the published version of the manuscript.

Funding: This research was funded by the Spanish Ministry of Economy, Industry and Competitiveness (MINECO-FEDER) through the projects CTM2016-75509-R and RTI2018-093310-B-I00 and by the State Research Agency (APCIN 2018) through the project X-MEM (PCI2018-092929).

Acknowledgments: Marta Romay is grateful to an FPI contract grant (BES-2017-081112).

Conflicts of Interest: The authors declare no conflict of interest.

References

1. Secretary-General of the United Nations. The Stockholm Convention on Persistant Organic Pollutants. 2009. Available online: http://chm.pops.int/TheConvention/Overview/TextoftheConvention/tabid/2232/ (accessed on 11 June 2019).
2. Dwivedi, A.H.; Pande, U.C. Photochemical Degradation of Halogenated Compounds: A Review. *Sci. Rev. Chem. Commun.* **2012**, *2*, 41–65.
3. Lee, S.Y.; Park, S.J. TiO_2 photocatalyst for water treatment applications. *J. Ind. Eng. Chem.* **2013**, *19*, 1761–1769. [CrossRef]
4. Zheng, X.; Shen, Z.-P.; Shi, L.; Cheng, R.; Yuan, D.-H.; Zheng, X.; Shen, Z.-P.; Shi, L.; Cheng, R.; Yuan, D.-H. Photocatalytic Membrane Reactors (PMRs) in Water Treatment: Configurations and Influencing Factors. *Catalysts* **2017**, *7*, 224. [CrossRef]

5. Iglesias, O.; Rivero, M.J.; Urtiaga, A.M.; Ortiz, I. Membrane-based photocatalytic systems for process intensification. *Chem. Eng. J.* **2016**, *305*, 136–148. [CrossRef]
6. Turan, N.B.; Erkan, S.; Engin, G.O.; Bilgili, S. Nanoparticles in the aquatic environment: Usage, properties, transformation and toxicity—A review. *Process Saf. Environ. Prot.* **2019**, *130*, 238–249. [CrossRef]
7. Kumari, P.; Bahadur, N.; Dumée, L.F. Photo-catalytic membrane reactors for the remediation of persistent organic pollutants—A review. *Sep. Purif. Technol.* **2020**, *230*, 115878. [CrossRef]
8. Mozia, S. Photocatalytic membrane reactors (PMRs) in water and wastewater treatment. A review. *Sep. Purif. Technol.* **2010**, *73*, 71–91. [CrossRef]
9. Janssens, R.; Mandal, M.K.; Dubey, K.K.; Luis, P. Slurry photocatalytic membrane reactor technology for removal of pharmaceutical compounds from wastewater: Towards cytostatic drug elimination. *Sci. Total Environ.* **2017**, *599–600*, 612–626. [CrossRef] [PubMed]
10. Wang, L. Configurations and Membranes of Photocatalytic Membrane Reactors for Water and Wastewater Treatment. In *IOP Conference Series: Earth and Environmental Science*; IOP Publishing: Bristol, UK, 2018; Volume 208.
11. Qing, W.; Li, X.; Shao, S.; Shi, X.; Wang, J.; Feng, Y.; Zhang, W.; Zhang, W. Polymeric catalytically active membranes for reaction-separation coupling: A review. *J. Memb. Sci.* **2019**, *583*, 118–138. [CrossRef]
12. Yin, J.; Deng, B. Polymer-matrix nanocomposite membranes for water treatment. *J. Memb. Sci.* **2015**, *479*, 256–275. [CrossRef]
13. Shi, Y.; Huang, J.; Zeng, G.; Cheng, W.; Hu, J. Photocatalytic membrane in water purification: Is it stepping closer to be driven by visible light? *J. Memb. Sci.* **2019**, *584*, 364–392. [CrossRef]
14. Riaz, S.; Park, S.J. An overview of TiO_2-based photocatalytic membrane reactors for water and wastewater treatments. *J. Ind. Eng. Chem.* **2020**. [CrossRef]
15. Méricq, J.-P.; Mendret, J.; Brosillon, S.; Faur, C. High performance PVDF-TiO_2 membranes for water treatment. *Chem. Eng. Sci.* **2015**, *123*, 283–291. [CrossRef]
16. Tran, D.T.; Mendret, J.; Méricq, J.P.; Faur, C.; Brosillon, S. Study of permeate flux behavior during photo-filtration using photocatalytic composite membranes. *Chem. Eng. Process.-Process Intensif.* **2020**, *148*, 107781. [CrossRef]
17. Chen, Q.; Yu, Z.; Pan, Y.; Zeng, G.; Shi, H.; Yang, X.; Li, F.; Yang, S.; He, Y. Enhancing the photocatalytic and antibacterial property of polyvinylidene fluoride membrane by blending Ag–TiO_2 nanocomposites. *J. Mater. Sci. Mater. Electron.* **2017**, *28*, 3865–3874. [CrossRef]
18. Wang, M.; Qu, F.; Jia, R.; Sun, S.; Li, G.; Liang, H. Preliminary study on the removal of steroidal estrogens using TiO_2 -doped PVDF ultrafiltration membranes. *Water* **2016**, *8*, 134. [CrossRef]
19. Sakarkar, S.; Muthukumaran, S.; Jegatheesan, V. Polyvinylidene Fluoride and Titanium Dioxide Ultrafiltration Photocatalytic Membrane: Fabrication, Morphology, and Its Application in Textile Wastewater Treatment. *J. Environ. Eng.* **2020**, *146*, 04020053. [CrossRef]
20. Xu, Z.; Wu, T.; Shi, J.; Teng, K.; Wang, W.; Ma, M.; Li, J.; Qian, X.; Li, C.; Fan, J. Photocatalytic antifouling PVDF ultrafiltration membranes based on synergy of graphene oxide and TiO_2 for water treatment. *J. Memb. Sci.* **2016**, *520*, 281–293. [CrossRef]
21. Zhang, J.; Xu, Z.; Shan, M.; Zhou, B.; Li, Y.; Li, B.; Niu, J.; Qian, X. Synergetic effects of oxidized carbon nanotubes and graphene oxide on fouling control and anti-fouling mechanism of polyvinylidene fluoride ultrafiltration membranes. *J. Memb. Sci.* **2013**, *448*, 81–92. [CrossRef]
22. Liu, Q.; Huang, S.; Zhang, Y.; Zhao, S. Comparing the antifouling effects of activated carbon and TiO_2 in ultrafiltration membrane development. *J. Colloid Interface Sci.* **2018**, *515*, 109–118. [CrossRef]
23. Song, H.; Shao, J.; He, Y.; Liu, B.; Zhong, X. Natural organic matter removal and flux decline with PEG–TiO_2-doped PVDF membranes by integration of ultrafiltration with photocatalysis. *J. Memb. Sci.* **2012**, *405–406*, 48–56. [CrossRef]
24. Song, H.; Shao, J.; Wang, J.; Zhong, X. The removal of natural organic matter with LiCl–TiO_2-doped PVDF membranes by integration of ultrafiltration with photocatalysis. *Desalination* **2014**, *344*, 412–421. [CrossRef]
25. Benhabiles, O.; Galiano, F.; Marino, T.; Mahmoudi, H.; Lounici, H.; Figoli, A. Preparation and Characterization of TiO_2-PVDF/PMMA Blend Membranes Using an Alternative Non-Toxic Solvent for UF/MF and Photocatalytic Application. *Molecules* **2019**, *24*, 724. [CrossRef] [PubMed]
26. Damodar, R.A.; You, S.-J.; Chou, H.-H. Study the self cleaning, antibacterial and photocatalytic properties of TiO_2 entrapped PVDF membranes. *J. Hazard. Mater.* **2009**, *172*, 1321–1328. [CrossRef]

27. Mungondori, H.H.; Tichagwa, L.; Katwire, D.M.; Aoyi, O. Preparation of photo-catalytic copolymer grafted asymmetric membranes (N-TiO_2-PMAA-g-PVDF/PAN) and their application on the degradation of bentazon in water. *Iran. Polym. J.* **2016**, *25*, 135–144. [CrossRef]
28. Jyothi, M.S.; Nayak, V.; Padaki, M.; Balakrishna, R.G.; Soontarapa, K. Eco-friendly membrane process and product development for complete elimination of chromium toxicity in wastewater. *J. Hazard. Mater.* **2017**, *332*, 112–123. [CrossRef]
29. Yang, Y.; Zhang, H.; Wang, P.; Zheng, Q.; Li, J. The influence of nano-sized TiO_2 fillers on the morphologies and properties of PSF UF membrane. *J. Memb. Sci.* **2007**, *288*, 231–238. [CrossRef]
30. Wang, Q.; Yang, C.; Zhang, G.; Hu, L.; Wang, P. Photocatalytic Fe-doped TiO_2/PSF composite UF membranes: Characterization and performance on BPA removal under visible-light irradiation. *Chem. Eng. J.* **2017**, *319*, 39–47. [CrossRef]
31. El-Aassar, A.; Hameed, M.; Isawi, H.; El-Noss, M.; El-Kholy, R.A.; Said, M.M.; Shawky, H.A. Design and fabrication of continuous flow photoreactor using semiconductor oxides for degradation of organic pollutants. *J. Water Process Eng.* **2019**, *32*, 100922. [CrossRef]
32. Kuvarega, A.T.; Khumalo, N.; Dlamini, D.; Mamba, B.B. Polysulfone/N,Pd co-doped TiO_2 composite membranes for photocatalytic dye degradation. *Sep. Purif. Technol.* **2018**, *191*, 122–133. [CrossRef]
33. Xu, H.; Ding, M.; Chen, W.; Li, Y.; Wang, K. Nitrogen–doped GO/TiO_2 nanocomposite ultrafiltration membranes for improved photocatalytic performance. *Sep. Purif. Technol.* **2018**, *195*, 70–82. [CrossRef]
34. Yu, S.; Wang, Y.; Sun, F.; Wang, R.; Zhou, Y. Novel mpg-C3N4/TiO_2 nanocomposite photocatalytic membrane reactor for sulfamethoxazole photodegradation. *Chem. Eng. J.* **2018**, *337*, 183–192. [CrossRef]
35. Muhulet, A.; Tuncel, C.; Miculescu, F.; Pandele, A.M.; Bobirica, C.; Orbeci, C.; Bobirica, L.; Palla-Papavlu, A.; Voicu, S.I. Synthesis and characterization of polysulfone–TiO_2 decorated MWCNT composite membranes by sonochemical method. *Appl. Phys. A Mater. Sci. Process.* **2020**, *126*, 233. [CrossRef]
36. Sotto, A.; Boromand, A.; Zhang, R.; Luis, P.; Arsuaga, J.M.; Kim, J.; Van der Bruggen, B. Effect of nanoparticle aggregation at low concentrations of TiO_2 on the hydrophilicity, morphology, and fouling resistance of PES–TiO_2 membranes. *J. Colloid Interface Sci.* **2011**, *363*, 540–550. [CrossRef] [PubMed]
37. Hoseini, S.N.; Pirzaman, A.K.; Aroon, M.A.; Pirbazari, A.E. Photocatalytic degradation of 2,4-dichlorophenol by Co-doped TiO_2 (Co/TiO_2) nanoparticles and Co/TiO_2 containing mixed matrix membranes. *J. Water Process Eng.* **2017**, *17*, 124–134. [CrossRef]
38. Safarpour, M.; Vatanpour, V.; Khataee, A. Preparation and characterization of graphene oxide/TiO_2 blended PES nanofiltration membrane with improved antifouling and separation performance. *Desalination* **2016**, *393*, 65–78. [CrossRef]
39. Zangeneh, H.; Zinatizadeh, A.A.; Zinadini, S.; Feyzi, M.; Bahnemann, D.W. Preparation and characterization of a novel photocatalytic self-cleaning PES nanofiltration membrane by embedding a visible-driven photocatalyst boron doped-TiO_2SiO_2/CoFe2O4 nanoparticles. *Sep. Purif. Technol.* **2019**, *209*, 764–775. [CrossRef]
40. Salim, N.E.; Jaafar, J.; Ismail, A.F.; Othman, M.H.D.; Rahman, M.A.; Yusof, N.; Qtaishat, M.; Matsuura, T.; Aziz, F.; Salleh, W.N.W. Preparation and characterization of hydrophilic surface modifier macromolecule modified poly (ether sulfone) photocatalytic membrane for phenol removal. *Chem. Eng. J.* **2018**, *335*, 236–247. [CrossRef]
41. Salim, N.E.; Nor, N.A.M.; Jaafar, J.; Ismail, A.F.; Qtaishat, M.R.; Matsuura, T.; Othman, M.H.D.; Rahman, M.A.; Aziz, F.; Yusof, N. Effects of hydrophilic surface macromolecule modifier loading on PES/O-g-C3N4 hybrid photocatalytic membrane for phenol removal. *Appl. Surf. Sci.* **2019**, *465*, 180–191. [CrossRef]
42. Sun, T.; Liu, Y.; Shen, L.; Xu, Y.; Li, R.; Huang, L.; Lin, H. Magnetic field assisted arrangement of photocatalytic TiO_2 particles on membrane surface to enhance membrane antifouling performance for water treatment. *J. Colloid Interface Sci.* **2020**, *570*, 273–285. [CrossRef]
43. Geng, Z.; Yang, X.; Boo, C.; Zhu, S.; Lu, Y.; Fan, W.; Huo, M.; Elimelech, M.; Yang, X. Self-cleaning anti-fouling hybrid ultrafiltration membranes via side chain grafting of poly(aryl ether sulfone) and titanium dioxide. *J. Memb. Sci.* **2017**, *529*, 1–10. [CrossRef]
44. Rajeswari, A.; Jackcina Stobel Christy, E.; Pius, A. New insight of hybrid membrane to degrade Congo red and Reactive yellow under sunlight. *J. Photochem. Photobiol. B Biol.* **2018**, *179*, 7–17. [CrossRef] [PubMed]
45. Rajeswari, A.; Vismaiya, S.; Pius, A. Preparation, characterization of nano ZnO-blended cellulose acetate-polyurethane membrane for photocatalytic degradation of dyes from water. *Chem. Eng. J.* **2017**, *313*, 928–937. [CrossRef]

46. Martins, P.M.; Ribeiro, J.M.; Teixeira, S.; Petrovykh, D.Y.; Cuniberti, G.; Pereira, L.; Lanceros-Méndez, S. Photocatalytic Microporous Membrane against the Increasing Problem of Water Emerging Pollutants. *Materials* **2019**, *12*, 1649. [CrossRef] [PubMed]
47. Aoudjit, L.; Martins, P.M.; Madjene, F.; Petrovykh, D.Y.; Lanceros-Mendez, S. Photocatalytic reusable membranes for the effective degradation of tartrazine with a solar photoreactor. *J. Hazard. Mater.* **2018**, *344*, 408–416. [CrossRef]
48. Teixeira, S.; Martins, P.M.; Lanceros-Méndez, S.; Kühn, K.; Cuniberti, G. Reusability of photocatalytic TiO_2 and ZnO nanoparticles immobilized in poly(vinylidene difluoride)-co-trifluoroethylene. *Appl. Surf. Sci.* **2016**, *384*, 497–504. [CrossRef]
49. Martins, P.M.; Miranda, R.; Marques, J.; Tavares, C.J.; Botelho, G.; Lanceros-Mendez, S. Comparative efficiency of TiO_2 nanoparticles in suspension vs. immobilization into P(VDF-TrFE) porous membranes. *RSC Adv.* **2016**, *6*, 12708–12716. [CrossRef]
50. Salazar, H.; Martins, P.M.; Santos, B.; Fernandes, M.M.; Reizabal, A.; Sebastián, V.; Botelho, G.; Tavares, C.J.; Vilas-Vilela, J.L.; Lanceros-Mendez, S. Photocatalytic and antimicrobial multifunctional nanocomposite membranes for emerging pollutants water treatment applications. *Chemosphere* **2020**, *250*, 126299. [CrossRef]
51. Melvin Ng, H.K.; Leo, C.P.; Abdullah, A.Z. Selective removal of dyes by molecular imprinted TiO_2 nanoparticles in polysulfone ultrafiltration membrane. *J. Environ. Chem. Eng.* **2017**, *5*, 3991–3998. [CrossRef]
52. Paredes, L.; Murgolo, S.; Dzinun, H.; Dzarfan Othman, M.H.; Ismail, A.F.; Carballa, M.; Mascolo, G. Application of immobilized TiO_2 on PVDF dual layer hollow fibre membrane to improve the photocatalytic removal of pharmaceuticals in different water matrices. *Appl. Catal. B Environ.* **2019**, *240*, 9–18. [CrossRef]
53. Dzinun, H.; Othman, M.H.D.; Ismail, A.F.; Puteh, M.H.; A. Rahman, M.; Jaafar, J.; Adrus, N.; Hashim, N.A. Antifouling behavior and separation performance of immobilized TiO_2 in dual layer hollow fiber membranes. *Polym. Eng. Sci.* **2018**, *58*, 1636–1643. [CrossRef]
54. Dzinun, H.; Othman, M.H.D.; Ismail, A.F.; Matsuura, T.; Puteh, M.H.; Rahman, M.A.; Jaafar, J. Stability study of extruded dual layer hollow fibre membranes in a long operation photocatalysis process. *Polym. Test.* **2018**, *68*, 53–60. [CrossRef]
55. Dzinun, H.; Othman, M.H.D.; Ismail, A.F.; Puteh, M.H.; Rahman, M.A.; Jaafar, J. Stability study of PVDF/TiO_2 dual layer hollow fibre membranes under long-term UV irradiation exposure. *J. Water Process Eng.* **2017**, *15*, 78–82. [CrossRef]
56. Dzinun, H.; Othman, M.H.D.; Ismail, A.F.; Puteh, M.H.; Rahman, M.A.; Jaafar, J. Photocatalytic degradation of nonylphenol using co-extruded dual-layer hollow fibre membranes incorporated with a different ratio of TiO_2/PVDF. *React. Funct. Polym.* **2016**, *99*, 80–87. [CrossRef]
57. Dzinun, H.; Othman, M.H.D.; Ismail, A.F.; Puteh, M.H.; Rahman, M.A.; Jaafar, J. Performance evaluation of co-extruded microporous dual-layer hollow fiber membranes using a hybrid membrane photoreactor. *Desalination* **2017**, *403*, 46–52. [CrossRef]
58. Galiano, F.; Song, X.; Marino, T.; Boerrigter, M.; Saoncella, O.; Simone, S.; Faccini, M.; Chaumette, C.; Drioli, E.; Figoli, A.; et al. Novel Photocatalytic PVDF/Nano-TiO_2 Hollow Fibers for Environmental Remediation. *Polymers* **2018**, *10*, 1134. [CrossRef]
59. Ong, C.S.; Lau, W.J.; Goh, P.S.; Ng, B.C.; Ismail, A.F. Investigation of submerged membrane photocatalytic reactor (sMPR) operating parameters during oily wastewater treatment process. *Desalination* **2014**, *353*, 48–56. [CrossRef]
60. Teow, Y.H.; Ahmad, A.L.; Lim, J.K.; Ooi, B.S. Preparation and characterization of PVDF/TiO_2 mixed matrix membrane via in situ colloidal precipitation method. *Desalination* **2012**, *295*, 61–69. [CrossRef]
61. Almeida, N.A.; Martins, P.M.; Teixeira, S.; Lopes da Silva, J.A.; Sencadas, V.; Kühn, K.; Cuniberti, G.; Lanceros-Mendez, S.; Marques, P.A.A.P. TiO_2/graphene oxide immobilized in P(VDF-TrFE) electrospun membranes with enhanced visible-light-induced photocatalytic performance. *J. Mater. Sci.* **2016**, *51*, 6974–6986. [CrossRef]
62. Cheng, J.; Pu, H. A facile method to prepare polyvinylidene fluoride composite nanofibers with high photocatalytic activity via nanolayer coextrusion. *Eur. Polym. J.* **2018**, *99*, 361–367. [CrossRef]
63. Huang, Y.; Huang, Q.; Xiao, C.; You, Y.; Zhang, C.; Liu, H. Supported Electrospun Ultrafine Fibrous Poly(tetrafluoroethylene)/ZnO Porous Membranes and their Photocatalytic Applications. *Chem. Eng. Technol.* **2018**, *41*, 656–662. [CrossRef]

64. Kang, W.; Ju, J.; He, H.; Li, F.; Tao, L.; Dong, Y.; Cheng, B. Photocatalytic Degradation Performance of TiO_2 /PTFE Membrane Catalyst to Methylene Blue. *Chem. Lett.* **2016**, *45*, 1440–1443. [CrossRef]
65. Blanco, M.; Monteserín, C.; Angulo, A.; Pérez-Márquez, A.; Maudes, J.; Murillo, N.; Aranzabe, E.; Ruiz-Rubio, L.; Vilas, J.L. TiO_2-Doped Electrospun Nanofibrous Membrane for Photocatalytic Water Treatment. *Polymers* **2019**, *11*, 747. [CrossRef] [PubMed]
66. Yar, A.; Haspulat, B.; Üstün, T.; Eskizeybek, V.; Avci, A.; Kamiş, H.; Achour, S. Electrospun TiO_2/ZnO/PAN hybrid nanofiber membranes with efficient photocatalytic activity. *RSC Adv.* **2017**, *7*, 29806–29814. [CrossRef]
67. Tissera, N.D.; Wijesena, R.N.; Sandaruwan, C.S.; de Silva, R.M.; de Alwis, A.; de Silva, K.M.M.N. Photocatalytic activity of ZnO nanoparticle encapsulated poly(acrylonitrile) nanofibers. *Mater. Chem. Phys.* **2018**, *204*, 195–206. [CrossRef]
68. Suriyaraj, S.P.; Benasir Begam, M.; Deepika, S.G.; Biji, P.; Selvakumar, R. Photocatalytic removal of nitrate using TiO_2/polyacrylonitrile nanofiber membrane synthesized by co-electrospinning process. *Water Sci. Technol. Water Supply* **2014**, *14*, 554–560. [CrossRef]
69. Jiang, Y.; Liu, D.; Cho, M.; Lee, S.S.; Zhang, F.; Biswas, P.; Fortner, J.D. In Situ Photocatalytic Synthesis of Ag Nanoparticles (nAg) by Crumpled Graphene Oxide Composite Membranes for Filtration and Disinfection Applications. *Environ. Sci. Technol.* **2016**, *50*, 2514–2521. [CrossRef]
70. Chen, Q.; Yu, Z.; Li, F.; Yang, Y.; Pan, Y.; Peng, Y.; Yang, X.; Zeng, G. A novel photocatalytic membrane decorated with RGO-Ag-$TiO_2$for dye degradation and oil–water emulsion separation. *J. Chem. Technol. Biotechnol.* **2018**, *93*, 761–775. [CrossRef]
71. Zhao, H.; Chen, S.; Quan, X.; Yu, H.; Zhao, H. Integration of microfiltration and visible-light-driven photocatalysis on g-C3N4 nanosheet/reduced graphene oxide membrane for enhanced water treatment. *Appl. Catal. B Environ.* **2016**, *194*, 134–140. [CrossRef]
72. Pastrana-Martínez, L.M.; Morales-Torres, S.; Figueiredo, J.L.; Faria, J.L.; Silva, A.M.T. Graphene oxide based ultrafiltration membranes for photocatalytic degradation of organic pollutants in salty water. *Water Res.* **2015**, *77*, 179–190. [CrossRef]
73. Xu, C.; Xu, Y.; Zhu, J. Photocatalytic antifouling graphene oxide-mediated hierarchical filtration membranes with potential applications on water purification. *ACS Appl. Mater. Interfaces* **2014**, *6*, 16117–16123. [CrossRef] [PubMed]
74. Xu, C.; Cui, A.; Xu, Y.; Fu, X. Graphene oxide–TiO_2 composite filtration membranes and their potential application for water purification. *Carbon N. Y.* **2013**, *62*, 465–471. [CrossRef]
75. Sun, K.; Wang, L.; Wu, C.; Deng, J.; Pan, K. Fabrication of α-Fe_2O_3 @rGO/PAN Nanofiber Composite Membrane for Photocatalytic Degradation of Organic Dyes. *Adv. Mater. Interfaces* **2017**, *4*, 1700845. [CrossRef]
76. Nair, A.K.; Jagadeesh, J.B. TiO_2 nanosheet-graphene oxide based photocatalytic hierarchical membrane for water purification. *Surf. Coat. Technol.* **2017**, *320*, 259–262. [CrossRef]
77. Gao, P.; Liu, Z.; Tai, M.; Sun, D.D.; Ng, W. Multifunctional graphene oxide–TiO_2 microsphere hierarchical membrane for clean water production. *Appl. Catal. B Environ.* **2013**, *138–139*, 17–25. [CrossRef]
78. Wu, T.; Zhang, Z.; Zhai, D.; Liu, Y.; Liu, Q.; Xue, L.; Gao, C.; Wu, T.; Zhang, Z.; Zhai, D.; et al. Dye Degrading and Fouling-Resistant Membranes Formed by Deposition with Ternary Nanocomposites of N-Doped Graphene/TiO_2/Activated Carbon. *Membranes* **2019**, *9*, 16. [CrossRef]
79. Aboamera, N.M.; Mohamed, A.; Salama, A.; Osman, T.A.; Khattab, A. An effective removal of organic dyes using surface functionalized cellulose acetate/graphene oxide composite nanofibers. *Cellulose* **2018**, *25*, 4155–4166. [CrossRef]
80. Mohamed, A.; Osman, T.A.; Toprak, M.S.; Muhammed, M.; Yilmaz, E.; Uheida, A. Visible light photocatalytic reduction of Cr(VI) by surface modified CNT/titanium dioxide composites nanofibers. *J. Mol. Catal. A Chem.* **2016**, *424*, 45–53. [CrossRef]
81. Shi, Y.; Yang, D.; Li, Y.; Qu, J.; Yu, Z.Z. Fabrication of PAN@TiO_2/Ag nanofibrous membrane with high visible light response and satisfactory recyclability for dye photocatalytic degradation. *Appl. Surf. Sci.* **2017**, *426*, 622–629. [CrossRef]
82. Gao, Y.; Hu, M.; Mi, B. Membrane surface modification with TiO_2–graphene oxide for enhanced photocatalytic performance. *J. Memb. Sci.* **2014**, *455*, 349–356. [CrossRef]
83. Jiang, R.; Wen, W.; Wu, J.M. Titania nanowires coated PEI/P25 membranes for photocatalytic and ultrafiltration applications. *New J. Chem.* **2018**, *42*, 3020–3027. [CrossRef]

84. You, S.-J.; Semblante, G.U.; Lu, S.-C.; Damodar, R.A.; Wei, T.-C. Evaluation of the antifouling and photocatalytic properties of poly(vinylidene fluoride) plasma-grafted poly(acrylic acid) membrane with self-assembled TiO_2. *J. Hazard. Mater.* **2012**, *237–238*, 10–19. [CrossRef] [PubMed]
85. Irani, E.; Amoli-Diva, M. Hybrid adsorption–photocatalysis properties of quaternary magneto-plasmonic ZnO/MWCNTs nanocomposite for applying synergistic photocatalytic removal and membrane filtration in industrial wastewater treatment. *J. Photochem. Photobiol. A Chem.* **2020**, *391*, 112359. [CrossRef]
86. Ramasundaram, S.; Son, A.; Seid, M.G.; Shim, S.; Lee, S.H.; Chung, Y.C.; Lee, C.; Lee, J.; Hong, S.W. Photocatalytic applications of paper-like poly(vinylidene fluoride)-titanium dioxide hybrids fabricated using a combination of electrospinning and electrospraying. *J. Hazard. Mater.* **2015**, *285*, 267–276. [CrossRef]
87. Xie, R.; Zhang, L.; Liu, H.; Xu, H.; Zhong, Y.; Sui, X.; Mao, Z. Construction of CQDs-Bi20TiO32/PAN electrospun fiber membranes and their photocatalytic activity for isoproturon degradation under visible light. *Mater. Res. Bull.* **2017**, *94*, 7–14. [CrossRef]
88. Nor, N.A.M.; Jaafar, J.; Ismail, A.F.; Mohamed, M.A.; Rahman, M.A.; Othman, M.H.D.; Lau, W.J.; Yusof, N. Preparation and performance of PVDF-based nanocomposite membrane consisting of TiO_2 nanofibers for organic pollutant decomposition in wastewater under UV irradiation. *Desalination* **2016**, *391*, 89–97. [CrossRef]
89. Fischer, K.; Kühnert, M.; Gläser, R.; Schulze, A. Photocatalytic degradation and toxicity evaluation of diclofenac by nanotubular titanium dioxide–PES membrane in a static and continuous setup. *RSC Adv.* **2015**, *5*, 16340–16348. [CrossRef]
90. Corredor, J.; Rivero, M.J.; Rangel, C.M.; Gloaguen, F.; Ortiz, I. Comprehensive review and future perspectives on the photocatalytic hydrogen production. *J. Chem. Technol. Biotechnol.* **2019**, *94*, 3049–3063. [CrossRef]
91. Koe, W.S.; Lee, J.W.; Chong, W.C.; Pang, Y.L.; Sim, L.C. An overview of photocatalytic degradation: Photocatalysts, mechanisms, and development of photocatalytic membrane. *Environ. Sci. Pollut. Res.* **2019**, *27*, 2522–2565. [CrossRef]
92. Yang, J.; Liu, B.; Zhao, X. A visible-light-active Au-Cu(I)@$Na_2Ti_6O_{13}$ nanostructured hybrid pasmonic photocatalytic membrane for acetaldehyde elimination. *Chin. J. Catal.* **2017**, *38*, 2048–2055. [CrossRef]
93. Fang, W.; Xing, M.; Zhang, J. Modifications on reduced titanium dioxide photocatalysts: A review. *J. Photochem. Photobiol. C Photochem. Rev.* **2017**, *32*, 21–39. [CrossRef]
94. Yi, H.; Huang, D.; Qin, L.; Zeng, G.; Lai, C.; Cheng, M.; Ye, S.; Song, B.; Ren, X.; Guo, X. Selective prepared carbon nanomaterials for advanced photocatalytic application in environmental pollutant treatment and hydrogen production. *Appl. Catal. B Environ.* **2018**, *239*, 408–424. [CrossRef]
95. Leary, R.; Westwood, A. Carbonaceous nanomaterials for the enhancement of TiO_2 photocatalysis. *Carbon* **2011**, *49*, 741–772. [CrossRef]
96. Sudhaik, A.; Raizada, P.; Shandilya, P.; Jeong, D.-Y.; Lim, J.-H.; Singh, P. Review on fabrication of graphitic carbon nitride based efficient nanocomposites for photodegradation of aqueous phase organic pollutants. *J. Ind. Eng. Chem.* **2018**, *67*, 28–51. [CrossRef]
97. Rahimpour, A.; Madaeni, S.S.; Taheri, A.H.; Mansourpanah, Y. Coupling TiO_2 nanoparticles with UV irradiation for modification of polyethersulfone ultrafiltration membranes. *J. Memb. Sci.* **2008**, *313*, 158–169. [CrossRef]
98. Fujishima, A.; Zhang, X. Titanium dioxide photocatalysis: Present situation and future approaches. *Comptes Rendus Chim.* **2006**, *9*, 750–760. [CrossRef]
99. Chin, S.S.; Chiang, K.; Fane, A.G. The stability of polymeric membranes in a TiO_2 photocatalysis process. *J. Memb. Sci.* **2006**, *275*, 202–211. [CrossRef]
100. Tsehaye, M.T.; Velizarov, S.; Van der Bruggen, B. Stability of polyethersulfone membranes to oxidative agents: A review. *Polym. Degrad. Stab.* **2018**, *157*, 15–33. [CrossRef]
101. Mulder, M. *Basic Principles of Membrane Technology*; Springer Science & Business Media: Twente, The Netherland, 1991; ISBN 0-7923-0978-2.
102. Aryanti, P.T.P.; Ariono, D.; Hakim, A.N.; Wenten, I.G. Flory-Huggins Based Model to Determine Thermodynamic Property of Polymeric Membrane Solution. *J. Phys.* **2018**, *1090*, 012074. [CrossRef]
103. Mohsenpour, S.; Esmaeilzadeh, F.; Safekordi, A.; Tavakolmoghadam, M.; Rekabdar, F.; Hemmati, M. The role of thermodynamic parameter on membrane morphology based on phase diagram. *J. Mol. Liq.* **2016**, *224*, 776–785. [CrossRef]

104. Bottino, A.; Camera-Roda, G.; Capannelli, G.; Munari, S. The formation of microporous polyvinylidene difluoride membranes by phase separation. *J. Memb. Sci.* **1991**, *57*, 1–20. [CrossRef]
105. Bassyouni, M.; Abdel-Aziz, M.H.; Zoromba, M.S.; Abdel-Hamid, S.M.S.; Drioli, E. A review of polymeric nanocomposite membranes for water purification. *J. Ind. Eng. Chem.* **2019**, *73*, 19–46. [CrossRef]
106. Mohamed, A.; Yousef, S.; Ali Abdelnaby, M.; Osman, T.A.; Hamawandi, B.; Toprak, M.S.; Muhammed, M.; Uheida, A. Photocatalytic degradation of organic dyes and enhanced mechanical properties of PAN/CNTs composite nanofibers. *Sep. Purif. Technol.* **2017**, *182*, 219–223. [CrossRef]
107. Li, X.; Sotto, A.; Li, J.; Van der Bruggen, B. Progress and perspectives for synthesis of sustainable antifouling composite membranes containing in situ generated nanoparticles. *J. Memb. Sci.* **2017**, *524*, 502–528. [CrossRef]
108. Molinari, R.; Lavorato, C.; Argurio, P. Recent progress of photocatalytic membrane reactors in water treatment and in synthesis of organic compounds. A review. *Catal. Today* **2017**, *281*, 144–164. [CrossRef]
109. Argurio, P.; Fontananova, E.; Molinari, R.; Drioli, E. Photocatalytic Membranes in Photocatalytic Membrane Reactors. *Processes* **2018**, *6*, 162. [CrossRef]
110. Horovitz, I.; Gitis, V.; Avisar, D.; Mamane, H. Ceramic-based photocatalytic membrane reactors for water treatment—Where to next? *Rev. Chem. Eng.* **2019**. [CrossRef]